NATIONAL ADVISORY COMMITTEE
FOR AERONAUTICS

TECHNICAL NOTE 3937

A COMPARISON OF TYPICAL NATIONAL GAS TURBINE ESTABLISHMENT

AND NACA AXIAL-FLOW COMPRESSOR BLADE SECTIONS

IN CASCADE AT LOW SPEED

By A. Richard Felix and James C. Emery

Langley Aeronautical Laboratory
Langley Field, Va.

NACA

Washington

March 1957

FOR REFERENCE

NATIONAL ADVISORY COMMITTEE FOR AERONAUTICS

3 1176 01434 0864

TECHNICAL NOTE 3937

A COMPARISON OF TYPICAL NATIONAL GAS TURBINE ESTABLISHMENT

AND NACA AXIAL-FLOW COMPRESSOR BLADE SECTIONS

IN CASCADE AT LOW SPEED[1]

By A. Richard Felix and James C. Emery

SUMMARY

Comparative low-speed cascade tests of the NGTE (National Gas Turbine Establishment of Great Britain) 10C4/30C50 and NACA 65-$(12A_{10})$10 axial-flow compressor blade sections were conducted at air-inlet angles of 30°, 45°, and 60° and a solidity of 1.0 by using the porous-wall technique. These tests indicated that the NGTE 10C4/30C50 and NACA 65-$(12A_{10})$10 sections have similar performance characteristics, that is, turning angles, drag coefficients, and operating ranges. Examination of the blade-surface pressure distributions indicated that the NACA 65-$(12A_{10})$10 section would have a slightly higher critical Mach number than the NGTE 10C4/30C50 section at or near design conditions.

The performance of the NGTE 10C4/30C50 axial-flow compressor blade section as given by NGTE design charts was compared with NACA tests of this section. Significant differences in turning angle were observed. These differences are attributed to the fact that NGTE tests were conducted in solid-wall tunnels and the NACA tests, in porous-wall tunnels.

Although there are differences between British and NACA force-analysis equations, for a given set of test results, the lift and drag coefficients obtained by using these equations agree closely.

INTRODUCTION

Inasmuch as both British and NACA axial-flow compressor blade sections are used in aircraft gas turbines constructed in this country, a performance comparison was desired between a typical NACA 65-series section having a constant-loading (a = 1.0) mean line and a typical British C4

---

[1]Supersedes recently declassified NACA Research Memorandum L53B26a by A. Richard Felix and James C. Emery, 1953.

section having a circular-arc mean line. For this comparison, the NACA
65-$(12A_{10})10$ and NGTE 10C4/30C50 sections were chosen since previous tests
indicated that these sections have similar lift coefficients at the
design angle of attack in cascade; the tests were made in a 5-inch low-
speed cascade tunnel at the Langley Laboratory by using the porous-wall
technique (ref. 1). The aim of these tests was to determine, within
the limitations of two-dimensional low-speed cascade tests, the rela-
tive merits of the aforementioned sections as to operating range, sur-
face pressures, and minimum drag values. A second objective was to
establish any differences between NACA and NGTE results attributable to
different tunnel effects and testing techniques. The test results for
the NGTE 10C4/30C50 section were obtained from references 2 and 3.

SYMBOLS

All symbols used in this paper are NACA symbols unless otherwise
indicated; however, for convenience both the NACA notation and the NGTE
notation are included in the list of symbols. Figure 1 presents a com-
parison of the notations used.

NACA		NGTE
A	aspect ratio	AR
b	blade span or height, ft	H
c	blade chord, ft	c
c_d	section drag coefficient	C_D
c_l	section lift coefficient	C_L
F	force, lb	
g	gap or pitch, ft	s
L/D	lift-drag ratio	L/D
M	Mach number	M_n
p	static pressure, lb/sq ft	P
P	total pressure, lb/sq ft	P_{tot}
ΔP	total pressure loss, lb/sq ft	ω

$\overline{\Delta P}$	mean total pressure loss, lb/sq ft	$\overline{\omega}$
q	dynamic pressure, lb/sq ft	q
R	Reynolds number	R_n
$C_p = \dfrac{P_1 - P_l}{q_1}$	pressure coefficient	
ΔC_p	incremental pressure coefficient	
t	blade maximum thickness, percent c	t
V	velocity, ft/sec	V
	normal velocity coefficient	v_n^*
α	angle of attack, deg	$i + x_1$
β	air angle, deg	α
ξ	blade setting angle, deg	ξ
$\theta = \beta_1 - \beta_2$	turning angle or deflection, deg	$\epsilon = \alpha_1 - \alpha_2$
ρ	mass density, slugs/cu ft	ρ
σ	solidity, $\dfrac{c}{g}$	
	blade mean-line angle, deg	β
	incidence, deg	$i = \alpha_1 - \beta_1$
	camber, deg	$\theta = x_1 + x_2$
	deviation, deg	$\delta = \alpha_2 - \beta_2$
	camber inlet angle, deg	x_1
	camber outlet angle, deg	x_2
	loading factor	ψ

Subscripts

a	axial component	a
M	momentum	
m	referred to vector mean velocity	m
R	relative to rotor blade	
θ	tangential component	w
1	upstream of blade row	1
2	downstream of blade row	2
p	pressure	
	incidence	i
d	design condition	
l	local condition	
o	isolated airfoil condition	
s	outside wake, free stream	
	infinite pitching condition, that is, isolated airfoil	∞
	optimum condition	opt
	stall condition	s

The superscript $*$ indicates the nominal condition.

AIRFOIL SECTION DESIGNATIONS

In the designation NACA 65-(12A$_{10}$)10, the first two digits, 65, refer to a particular thickness distribution; the second two digits, 12, indicate the isolated airfoil lift coefficient in tenths; the A$_{10}$ describes the loading distribution (ref. 4); and the third pair of digits, 10, denotes the maximum thickness in percent chord.

In the designation NGTE 10C4/30C50, the first two digits, 10, denote the maximum thickness in percent chord; C4 indicates a thickness distribution; 30 indicates camber angle in degrees; C refers to the type of mean line, in this case, circular arc; and 50 is the distance of the point of maximum camber from the leading edge in percent chord.

TEST APPARATUS

Tunnel Configurations

The equipment used in these tests was a 5-inch low-speed cascade tunnel at the Langley Laboratory described in reference 1. A description and layout of a typical NGTE low-speed cascade tunnel is presented in reference 5. NGTE and NACA low-speed cascade tunnels are similar in general layout. Almost all these tunnels discharge to the atmosphere and are powered by variable-speed centrifugal or axial blowers. Honeycombs are used to remove any swirl from the air, and screens are installed in the settling chamber to insure a uniform velocity distribution entering the test section. The NGTE cascades have contraction ratios entering the test section of between 7:1 and 12:1; whereas the ratios are between 20:1 and 40:1 in the NACA tunnels. The important differences between NGTE and NACA low-speed cascade tunnels are in the region of the test section. The porous-wall technique is employed in the NACA low-speed cascade tunnels. The side walls (fig. 2) are porous in the test section and are fitted with slots 1 chord upstream of the blades. Flexible porous end walls (fig. 2) are used in the test section and rigid porous end walls are used ahead of the blading. Since the boundary layer on the side walls had a greater distance to travel near one end wall than the other, a porous triangular inlet-air-angle plate is installed at inlet air angles of 45° or more. The NGTE tunnels use only suction slots between each of the end blades and the end walls for removing the boundary layer (ref. 5).

A seven-blade cascade is the arrangement usually used at NACA, but a larger number of blades, usually about 13, is used by NGTE. Blade chords are similar; NACA uses 5-inch chords and NGTE, 4-inch chords. It has been shown in reference 1 that, in a porous-wall tunnel, results independent of aspect ratio can be obtained. Therefore, for conservation of power and convenience of manufacture, NACA cascade blades usually have an aspect ratio of 1.0. The NGTE blades ordinarily have an aspect ratio of 4.0.

The yaw probes most frequently used in both the NACA and NGTE tunnels are of the claw type and, more recently, the prism or arrowhead type (ref. 6). The common multitube total-pressure rake is used in the NACA tunnels for measuring losses, whereas a single total-pressure tube

coupled with an electric pressure recorder is used in the NGTE tunnels.
In both NACA and NGTE cascade testing, pressures and air angles are ordi-
narily measured at midspan. The accuracy of the measured air angles is
±0.25°.

Reynolds Number

The Reynolds numbers of most of the NACA and NGTE low-speed cascade
tests, based on blade chords and inlet velocities, fall roughly in the
range from 1.5×10^5 to 5.0×10^5. Because of the widely varying turbu-
lence levels of various cascade tunnels, effective Reynolds number is
frequently used when data from different tunnels are being compared.
Effective Reynolds number is defined as the measured Reynolds number
based on blade chord and inlet velocity times the turbulence factor
(ref. 7). Hot-wire anemometer measurements in the low-speed cascade
tunnels at the Langley Laboratory indicated turbulence levels of 0.4 per-
cent of the free-stream velocity and less. The corresponding turbulence
factor is about 1.2 (ref. 8). From sphere tests, it was determined that
the turbulence factor of the NGTE low-speed cascades is near 2.0 (ref. 7).
The tests made in the 5-inch low-speed cascade tunnel for this report
were run at effective Reynolds numbers near 2.8×10^5; whereas the NGTE
tests from reference 2 were run at effective Reynolds numbers near
4.0×10^5.

RESULTS AND DISCUSSION

Comparison of Performance Characteristics of the NGTE

and NACA Axial-Flow Compressor Blade Sections

The comparative tests of the NGTE $10C4/30C50$ and NACA $65\text{-}(12A_{10})10$
sections were conducted in the 5-inch low-speed cascade tunnel at the
Langley Laboratory at air-inlet angles of 30°, 45°, and 60° and a
solidity of 1.0 by using the porous-wall technique. Ordinates of the
$10C4/30C50$ and $65\text{-}(12A_{10})10$ sections (fig. 3) are shown in tables I
and II, respectively. The similarity of the 30° circular-arc mean line
and the constant-loading (a = 1.0) mean line cambered for an isolated
airfoil lift coefficient of 1.2 may be seen in figure 4. The maximum
divergence between the two mean lines is 0.7 percent chord and occurs
at the 10-percent- and 90-percent-chord stations.

Turning angles and drag coefficients are plotted against angle of
attack for air-inlet angles of 30°, 45°, and 60° in figures 5, 6, and 7.
The angle-of-attack scales for the two blades have been shifted so that

the design angles of attack are alined. These design angles of attack
were chosen by the NACA method of inspecting the blade-surface pressure
distributions (ref. 9). In general, the turning angles and drag coef-
ficients of the two blade sections compare closely at the conditions
tested. Operating range is defined as the angle-of-attack range within
which the drag coefficient is twice the minimum value or less. The drag
curves indicate that both sections have a broad operating range of about
23° at $\beta = 30^{\circ}$, 20° at $\beta_1 = 45^{\circ}$, and 18° at $\beta_1 = 60^{\circ}$; the low minimum
drag values indicate efficient section operation. The irregularities in
the drags of both blades near the design angle of attack at $\beta_1 = 30^{\circ}$
and 60° are the results of the separation of a laminar boundary layer on
the convex surface (ref. 9).

Comparison of blade-surface pressure distributions near the design
turning angle at the air-inlet angles of 30°, 45°, and 60° are presented
in figures 8, 9, and 10, respectively. On both the convex and concave
surfaces, the NGTE section has higher peak pressure coefficients than
the NACA section because of the greater thickness of the NGTE section
near the leading edge; this fact indicates that the NACA 65-$(12A_{10})$10
section would have a higher critical Mach number than the NGTE 10C4/30C50
section.

As a further comparison, the change in blade-surface pressures with
a change in angle of attack at several chordwise stations was plotted
for both the concave and convex surfaces of the NACA 65-$(12A_{10})$10 and
NGTE 10C4/30C50 blade sections. The incremental pressure coefficient
ΔC_p is defined as the difference in the pressure coefficient C_p at
some angle of attack and $C_{p,d}$ at the design angle of attack. These
plots were made for the same conditions of air-inlet angle and solidity
as the preceding comparisons. Figures 11 to 14 present typical relations
between ΔC_p and α at the 10- and 60-percent-chord stations. The
relationship is approximately linear and can be represented by a slope
$\Delta C_p/\Delta \alpha$. The chordwise variation of this slope on both surfaces of the
NACA 65-$(12A_{10})$10 and NGTE 10C4/30C50 blade sections is shown in fig-
ures 15 and 16. The data presented in figures 11 to 16 include several
points obtained from cascade tests conducted at an effective Reynolds
number near 500,000 as well as data previously presented. There is no
effect of air-inlet angle on $\Delta C_p/\Delta \alpha$ over the first 10 percent of the
convex surface of the NACA 65-$(12A_{10})$10 blade section (fig. 15). Rear-
ward of the 10-percent-chord station, the effect of air-inlet angle
becomes very noticeable on the convex surface; $\Delta C_p/\Delta \alpha$ is decreased as
the air-inlet angle is increased. On the convex surface of the NGTE
10C4/30C50 blade section an effect of air-inlet angle becomes apparent
rearward of the 7.5-percent-chord station, whereas on the concave sur-
face the air-inlet angle changes did not affect $\Delta C_p/\Delta \alpha$. A comparison

of figures 15 and 16 indicate that, over the first 40 percent of the
convex surface where the highest velocities occur near design angle of
attack, the $\Delta C_p/\Delta \alpha$ values of the NGTE and the NACA sections agree
within 10 percent. Thus, the incremental velocities due to angle-of-
attack effects are similar for these sections despite their differences
in leading-edge radius, thickness distribution, and mean-line shapes.

Figures 15 and 16 may be used in conjunction with the design blade-
surface pressure distributions in figures 8, 9, and 10 to predict blade-
surface pressure distributions for air-inlet angles between 30° and 60°
at any nonstalled angle of attack. If the desired blade-surface pres-
sure distribution is for air-inlet angles of 30°, 45°, or 60°, the
$\Delta C_p/\Delta \alpha$ values in figures 15 or 16, depending on which blade section is
being used, can be applied directly to figures 8, 9, and 10. If, how-
ever, the desired data are for air-inlet angles other than 30°, 45°, or
60°, an interpolation must be performed to obtain the design blade-
surface pressure distribution. Then the $\Delta C_p/\Delta \alpha$ values are applied as
in the former case to find the off-design blade-surface pressure
distributions.

As previously pointed out, the NACA 65-$(12A_{10})10$ and NGTE 10C4/30C50
blade sections produce like turning angles at their design angles of
attack; this fact indicates the similarity of the effective cambers of
the NACA constant-loading mean line and the circular-arc mean line. The
agreement of the drag curves shows the similar profile-loss character-
istics of the two basic thickness distributions, the NACA 65-series and
the NGTE C4. Since the variation of the incremental pressure coefficient
with angle of attack is similar for the two blade sections, it appears
that, near critical speeds, the design blade-surface pressure distribu-
tions are the most important difference between the NACA 65-$(12A_{10})10$
and the NGTE 10C4/30C50 sections.

Comparison of NGTE and NACA Low-Speed Cascade Tests

of the NGTE 10C4/30C50 Section

At the National Gas Turbine Establishment a cascade having one com-
bination of solidity and camber is tested through a range of angles of
attack with the blade setting angle held constant, whereas at the National
Advisory Committee for Aeronautics the air-inlet angle is held constant
for the tests. Therefore, in order to compare the data for the NGTE
10C4/30C50 section, as reported in references 2 and 3, with NACA tests
of the same section at air-inlet angles of 30°, 45°, and 60° and a
solidity of 1.0, the NGTE data were recalculated and replotted to make
them comparable with the NACA tests. The methods used in recalculating
the data from references 2 and 3 are presented in appendix A. (A

comparison of the NACA and British incompressible cascade force-analysis equations is presented in appendix B.)

Graphs of angle of attack against turning angle and drag coefficient were plotted for each of the air-inlet angles tested and are presented in figures 17, 18, and 19. At an air-inlet angle of 30° (fig. 17) the slopes of the curves of angle of attack plotted against turning angle for both sets of data are similar. The turning angles from the NGTE data are consistently about 2° higher than the NACA test results near the design angle of attack. The drag curves show fair agreement as to minimum values and operating range. The drag curve from the NACA tests indicates some laminar separation at low angles of attack.

At an air-inlet angle of 45° (fig. 18), the NGTE turning angles are slightly higher than the NACA angles throughout most of the angle-of-attack range. The maximum difference near design angle of attack is about 1.7°. The drag curves have similar minimum values although the NACA test data indicate a slightly wider operating range than the NGTE data.

At an air-inlet angle of 60° (fig. 19), the slopes of the curves of angle of attack plotted against turning angle for both sets of data became somewhat divergent. As was the case at the other air-inlet angles, the NGTE turning angles are greater than the NACA turning angles, but at this condition the differences become exaggerated, particularly at the higher angles of attack. These differences are corroborated in reference 1 which indicates that the turning angle in a solid-wall tunnel at $A = 1.0$ agrees well with the porous-wall data but that the turning angle increases as the aspect ratio increases. Almost all the NGTE low-speed cascade tests are conducted with blades having $A = 2.0$ or more; therefore, turning angles greater than the porous-wall turning angles are to be expected. The drag values from the NGTE data indicate a slightly lower minimum drag coefficient than the NACA test results. However, laminar separation has affected the NACA drag values in the region of the design angle of attack. Test data from reference 1 indicate that, at low speeds, drag decreases with increasing Reynolds number; therefore, care must be exercised in comparing drag coefficients from low-speed cascade tests in various tunnels having different turbulence factors.

CONCLUDING REMARKS

Low-speed cascade tests at air-inlet angles of 30°, 45°, and 60° and a solidity of 1.0 made by using the porous-wall technique indicate that the NGTE 10C4/30C50 and the NACA 65-$(12A_{10})$10 axial-flow compressor blade sections have similar performance characteristics. Blade-surface

pressure distributions indicated that the NACA 65-(12A$_{10}$)10 section would have a slightly higher critical Mach number than the NGTE 10C4/30C50 section.

The performance characteristics of the NGTE 10C4/30C50 section as indicated by NACA tests show fair agreement with NGTE data at air-inlet angles of 30°, 45°, and 60° and a solidity of 1.0. The NGTE turning angles are, in general, slightly higher than the NACA angles at the conditions tested, the greatest differences occurring at an air-inlet angle of 60°. The maximum difference near design angle of attack is of order of 3.0°. These differences are attributed to the fact that the NGTE tests are conducted in solid-wall tunnels and the NACA tests in porous-wall tunnels. Data comparing NACA porous-wall and solid-wall low-speed cascade tests show differences similar to those found in the present tests.

Langley Aeronautical Laboratory,
      National Advisory Committee for Aeronautics,
            Langley Field, Va., February 27, 1953.

APPENDIX A

RECALCULATION OF NGTE DATA

In this appendix, the deflection ϵ and the drag coefficient C_D are to be calculated from data in references 2 and 3 when the blade setting angle ξ, the pitch-chord ratio s/c, and the air-inlet angle α_1 have been assumed. NGTE symbols are used throughout appendix A.

Recalculation of Data From Reference 2

The conditions to be assumed are as follows:

Airfoil . . . . NGTE 10C4/30C50
Blade setting angle, ξ, deg . . . . -26
Pitch-chord ratio, s/c 1.0
Blade inlet angle, β_1, deg 41
Blade outlet angle, β_2, deg 11
Air-inlet angle, α_1, deg 45
Incidence, i, deg 4

The deviation is given by

$$\delta = m\theta\sqrt{s/c}$$

where m is a function of the blade setting angle and the position of maximum camber (fig. 6 of ref. 2); therefore,

$$\delta = 0.255 \times 30 \times 1.0 = 7.7^\circ$$

Since $\delta = \alpha_2 - \beta_2$,

$$\alpha_{2,opt} = \beta_2 + \delta$$

$$= 11 + 7.7$$

$$= 18.7^\circ$$

The next step is to find the optimum incidence i_{opt} by a method of successive approximations as in appendix II of reference 2.

First approximation.- Let

$$i_{opt} = 0^o$$

then

$$\alpha_{1,opt} = 41^o$$

$$\alpha_{2,opt} = 18.7^o$$

and, by definition,

$$\epsilon_{opt} = \alpha_{1,opt} - \alpha_{2,opt}$$

$$= 41 - 18.7$$

$$= 22.3^o$$

Thus, by definition,

$$\tan \alpha_{m,opt} = \frac{1}{2}\left(\tan \alpha_{1,opt} + \tan \alpha_{2,opt}\right)$$

$$= \frac{1}{2}\left(0.869 + 0.338\right)$$

$$= 0.603$$

and

$$\alpha_{m,opt} = 31.1^o$$

From reference 7 (the C_D term being neglected),

$$C_{L,opt} = 2\frac{s}{c}\left(\tan \alpha_{1,opt} - \tan \alpha_{2,opt}\right)\cos \alpha_{m,opt}$$

$$= 2 \times 1.0(0.869 - 0.338)0.856$$

$$= 2 \times 0.531 \times 0.856$$

$$= 0.909$$

From reference 2,

$$i_{opt} = \Delta i + i_{opt,\infty}$$

From figure 5 of reference 2,

$$i_{opt,\infty} = -4.75^\circ$$

and from figure 2 of reference 2,

$$v_n{}^* = 0.151$$

and

$$\Delta i = \frac{v_n{}^* C_L}{2\frac{s}{c}} \; 57.3$$

$$= \frac{0.151 \times 0.909 \times 57.3}{2 \times 1.0}$$

$$= 3.91^\circ$$

and

$$i_{opt} = 3.91 - 4.75$$

$$= -0.84^\circ$$

as compared with the assumed value of 0°.

Second approximation.- Let

$$i_{opt} = -1.0^\circ$$

then

$$\alpha_{1,opt} = 40.0^\circ$$

$$\alpha_{2,opt} = 18.7^\circ$$

and, by definition,

$$\epsilon_{opt} = 40.0 - 18.7$$

$$= 21.3^\circ$$

Thus,

$$\tan \alpha_{m,opt} = \frac{1}{2}(0.839 + 0.338)$$

$$= 0.588$$

and

$$\alpha_{m,opt} = 30.4°$$

Using the equation for $C_{L,opt}$ from reference 7 and the preceding values yields

$$C_{L,opt} = 2 \times 1.0(0.839 - 0.338)0.862$$

$$= 2 \times 0.501 \times 0.862$$

$$= 0.864$$

Thus, from reference 2,

$$i_{opt,\infty} = -4.75°$$

Therefore,

$$\Delta i = \frac{0.151 \times 0.864 \times 57.3}{2 \times 1.0}$$

$$= 3.75°$$

and

$$i_{opt} = 3.75 - 4.75$$

$$= -1.0°$$

as compared with the assumed value of -1.0°.

The loading or lift coefficient based on outlet velocity is designated ψ in reference 2 and is equal to $C_L\left(\dfrac{\cos \alpha_2}{\cos \alpha_m}\right)^2$ (see ref. 10).

Therefore,

$$\psi_{opt} = C_{L,opt}\left(\frac{\cos \alpha_{2,opt}}{\cos \alpha_{m,opt}}\right)^2$$

$$= 0.864\left(\frac{0.947}{0.862}\right)^2$$

$$= 1.044$$

From reference 2,

$$\psi_{opt,\infty} = \psi_{opt}\frac{6s/c}{6\frac{s}{c} - 1}$$

$$= 1.044 \times 1.2$$

$$= 1.254$$

From figure 19 of reference 2,

$$i_s - i_{opt} = 6.8^\circ$$

and

$$\frac{i - i_{opt}}{i_s - i_{opt}} = \frac{4 - (-1.0)}{6.8}$$

$$= \frac{5.0}{6.8}$$

$$= 0.735$$

From figure 20 of reference 2,

$$\frac{\epsilon - \epsilon_{opt}}{i_s - i_{opt}} = 0.610$$

Solving for ϵ yields

$$\epsilon - 21.3 = 0.610 \times 6.8$$

$$\epsilon = 21.3 + 4.1$$

$$\epsilon = 25.4$$

By definition,

$$\alpha_2 = \alpha_1 - \epsilon$$

Thus, by substitution,

$$\alpha_2 = 45 - 25.4$$

$$= 19.6^{\circ}$$

From figure 14 of reference 2 for the values of $\alpha_{2,opt}$ and ϵ_{opt} previously calculated,

$$\left(\frac{L}{D}\right)_{opt} = 60$$

and

$$C_{D,opt} = \frac{C_{L,opt}}{\left(\dfrac{L}{D}\right)_{opt}}$$

$$= \frac{0.864}{60}$$

$$= 0.0144$$

Thus, by definition,

$$\tan \alpha_m = \frac{1}{2}\left(\tan \alpha_1 + \tan \alpha_2\right)$$

$$= \frac{1}{2}(1.000 + 0.356)$$

$$= 0.678$$

and

$$\alpha_m = 34.1°$$

From figure 20 of reference 2 the ratio of $\bar{\omega}$ to $\bar{\omega}$ at i_{opt} is given as

$$\frac{\bar{\omega}}{(\bar{\omega})_{i_{opt}}} = 1.330$$

By definition,

$$\frac{C_D}{C_{D,opt}} = \frac{\bar{\omega}}{(\bar{\omega})_{i_{opt}}} \frac{\cos \alpha_m}{\cos \alpha_{m,opt}}$$

$$= 1.330 \times \frac{0.828}{0.862}$$

$$= 1.278$$

By substitution,

$$C_D = 1.278 \times 0.0144$$

$$= 0.0184$$

and

$$C_{D,1} = C_D\left(\frac{\cos \alpha_1}{\cos \alpha_m}\right)^2$$

$$= 0.0184\left(\frac{0.707}{0.828}\right)^2$$

$$= 0.0134$$

Recalculation of Data From Reference 3

The conditions to be assumed are as follows:

Airfoil . . . . NGTE 10C4/30C50
Blade setting angle, ξ, deg . . . . -51
Pitch-chord ratio, s/c 1.0
Blade inlet angle, β_1, deg 66
Blade outlet angle, β_2, deg 36
Air-inlet angle, α_1, deg 60
Incidence, i, deg . . . . -6

It was necessary to cross-plot the data from reference 3 in order to obtain nominal incidences and nominal turning angles at intermediate air-outlet angles. Figure 20 is a plot of nominal incidence against air-outlet angle and figure 21 is a plot of nominal deflection against air-outlet angle.

First approximation.- Let

$$\alpha_2 = 46.0^\circ$$

then from figure 20,

$$i^* = -0.7^\circ$$

and from figure 21,

$$\epsilon^* = 19.5^\circ$$

Thus,

$$\frac{i - i^*}{\epsilon^*} = \frac{-6 - (-0.7)}{19.5}$$

$$= \frac{-5.3}{19.5}$$

$$= -0.272$$

From figure 9 of reference 11,

$$\frac{\epsilon}{\epsilon^*} = 0.740$$

By substitution,

$$\epsilon = 0.740 \times 19.5$$

$$= 14.4^{\circ}$$

and, by definition,

$$\alpha_2 = \alpha_1 - \epsilon$$

$$= 60 - 14.4$$

$$= 45.6^{\circ}$$

as compared with the assumed value of 46.0°.

Second approximation.- Let

$$\alpha_2 = 45.4^{\circ}$$

then from figure 20,

$$i^* = -0.8^{\circ}$$

and from figure 21,

$$\epsilon^* = 19.5^{\circ}$$

Thus,

$$\frac{i - i^*}{\epsilon^*} = \frac{-6 - (-0.8)}{19.5}$$

$$= -\frac{5.2}{19.5}$$

$$= -0.267$$

From figure 9 of reference 11,

$$\frac{\epsilon}{\epsilon^*} = 0.745$$

By substitution,

$$\epsilon = 0.745 \times 19.5$$

$$= 14.5^{\circ}$$

and, by definition,

$$\alpha_2 = \alpha_1 - \epsilon$$

$$= 60 - 14.5$$

$$= 45.5^{\circ}$$

as compared with the assumed value of 45.4°.

Then, by definition,

$$\tan \alpha_m = \frac{1}{2}\left(\tan \alpha_1 + \tan \alpha_2\right)$$

$$= \frac{1}{2}(1.732 + 1.016)$$

$$= 1.374$$

and

$$\alpha_m = 54.0^{\circ}$$

From figure 9 of reference 11,

$$C_D = 0.0213$$

and

$$C_{D,1} = 0.0213\left(\frac{\cos \alpha_1}{\cos \alpha_m}\right)^2$$

$$= 0.0213\left(\frac{0.5}{0.588}\right)^2$$

$$= 0.0213 \times 0.724$$

$$= 0.0154$$

APPENDIX B

INCOMPRESSIBLE CASCADE FORCE-ANALYSIS EQUATIONS

The two-dimensional resultant force on a blade in cascade is the vector sum of all the pressure and momentum forces exerted by the fluid. The NACA force equations consider two forces to act on a blade in the axial direction - the pressure force due to the pressure rise across the cascade and the momentum force due to the axial-velocity change. (NACA symbols are used throughout this appendix.) These equations as obtained from reference 9 are

$$F_p = \left(p_2 - p_1\right)bg \tag{1}$$

$$F_{M,a} = \rho V_{a,1}\left(V_{a,2,s} - V_{a,1}\right)bg + \int_g \rho V_{a,2}b\left(V_{a,2} - V_{a,2,s}\right)dg \tag{2}$$

The momentum force is the sum of momentum changes measured in the wake and in the free stream. In the axial direction the British system (ref. 7) shows a pressure force computed from the measured air angles and the mean total pressure loss across the passage $\overline{\Delta P}$. Since the axial velocity V_a is assumed to be constant, there is no momentum force in the axial direction and (from ref. 7)

$$F_p = \left(p_2 - p_1\right)bg$$

$$= \left[\frac{1}{2}\rho\left(V_{1,R}^2 - V_{2,R}^2\right) - \overline{\Delta P}\right]bg$$

$$= \left[\frac{1}{2}\rho V_a^2\left(\tan^2\beta_1 - \tan^2\beta_2\right) - \overline{\Delta P}\right]bg \tag{3}$$

In the tangential direction, the NACA equation shows a momentum force which is the sum of the momentum forces in the wake and free stream due to the change in tangential velocity and is (from ref. 9)

$$F_{M,\theta} = \rho V_{a,1}\left(V_{\theta,1,R} - V_{\theta,2,R,s}\right)bg + \int_g \rho V_{a,2}{}^b\left(V_{\theta,2,R,s} - V_{\theta,2,R}\right)dg$$

$$(4)$$

In the British system the tangential force is derived from the measured air angles and is (from ref. 7)

$$F_{M,\theta} = \rho V_a\left(V_{\theta,1,R} - V_{\theta,2,R}\right)bg = \rho V_a{}^2\left(\tan \beta_1 - \tan \beta_2\right)bg \qquad (5)$$

When the axial and tangential forces are known, the resultant blade force may be found and, subsequently, the lift and drag forces. In both systems the lift and drag forces are the components of the resultant blade force perpendicular and parallel to the vector mean velocity, respectively (ref. 9). It is also to be noted that the British lift and drag coefficients are based on q_m; whereas the NACA coefficients are based on q_1. In order to check the agreement of the forces computed by the British and NACA equations, several sets of cascade conditions including turning angles and wake shapes were assumed. For the assumed values, lift and drag coefficients based on q_1 were computed by both British and NACA equations with the results presented in the following table:

	$\beta_1 = 45^\circ$		$\beta_1 = 60^\circ$	
	c_l	c_d	c_l	c_d
$\sigma = 1.0$; $\theta = 20^\circ$				
NACA	0.627	0.0440	0.708	0.0122
NGTE	.627	.0469	.711	.0132
$\sigma = 1.0$; $\theta = 25^\circ$				
NACA	0.742	0.0350	0.794	0.0152
NGTE	.745	.0383	.792	.0160

The British equations indicate slightly higher drag coefficients than the NACA equations (by 5 to 10 percent), the lift coefficients being in good agreement.

REFERENCES

1. Erwin, John R., and Emery, James C.: Effect of Tunnel Configuration and Testing Technique on Cascade Performance. NACA Rep. 1016, 1951. (Supersedes NACA TN 2028.)

2. Carter, A. D. S.: The Low Speed Performance of Related Aerofoils in Cascades. C.P. No. 29 (Tech. Rep. No. 12,883), British A.R.C., 1950.

3. Carter, A. D. S., and Hounsell, A. F.: General Performance Data for Aerofoils Having C.1, C.2, or C.4 Base Profiles on Circular Arc Camber Lines. National Gas Turbine Establishment Memo. No. M.62, British Ministry of Supply, Aug. 1949.

4. Erwin, John R., and Yacobi, Laura A.: Method of Estimating the Incompressible-Flow Pressure Distribution of Compressor Blade Sections at Design Angle of Attack. NACA RM L53F17, 1953.

5. Carter, A. D. S., Andrews, S. J., and Shaw, H.: Some Fluid Dynamic Research Techniques. Proc. Inst. Mech. Eng. (London), vol. 163, 1950, pp. 249-263.

6. Schulze, Wallace M., Ashby, George C., Jr., and Erwin, John R.: Several Combination Probes for Surveying Static and Total Pressure and Flow Direction. NACA TN 2830, 1952.

7. Howell, A. R.: The Present Basis of Axial Flow Compressor Design. Part I. Cascade Theory and Performance. R. & M. No. 2095, British A.R.C., 1942.

8. Dryden, H. L., and Kuethe, A. M.: Effect of Turbulence in Wind Tunnel Measurements. NACA Rep. 342, 1930.

9. Herrig, L. Joseph, Emery, James C., and Erwin, John R.: Systematic Two-Dimensional Cascade Tests of NACA 65-Series Compressor Blades at Low Speeds. NACA TN 3916, 1956. (Supersedes NACA RM L51G31.)

10. Howell, A. R., and Carter, A. D. S.: Fluid Flow Through Cascades of Aerofoils. National Gas Turbine Establishment Rep. No. R.6, British Ministry of Supply, Sept. 1946.

11. Howell, A. R., and Bonham, R. P.: Overall and Stage Characteristics of Axial-Flow Compressors. Proc. Inst. Mech. Eng. (London), vol. 163, 1950, pp. 235-248.

TABLE I

ORDINATES FOR NGTE 10C4/30C50 SECTION

[Stations and ordinates in percent of chord]

Convex surface		Concave surface	
Station x	Ordinate y	Station x	Ordinate y
0	0	0	0
.834	1.925	1.666	-1.268
1.942	2.858	3.058	-1.543
4.283	4.265	5.717	-1.726
6.707	5.428	8.293	-1.637
9.168	6.330	10.832	-1.535
14.175	7.862	15.825	-1.088
19.250	9.014	20.750	-.529
29.483	10.520	30.517	.573
39.747	11.209	40.253	1.442
50.000	11.154	50.000	2.014
60.210	10.370	59.790	2.281
70.349	8.899	69.651	2.195
80.394	6.752	79.606	1.733
90.331	3.963	89.669	.832
95.247	2.300	94.753	.239
100.000	0	100.000	0

L.E. radius = 1.200   Slope through L.E. radius = 0.2680
T.E. radius = 0.600   Slope through T.E. radius = -0.2680
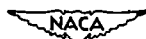
TABLE II

ORDINATES FOR NACA 65-(12A$_{10}$)10 SECTION

$$\left[\text{Stations and ordinates in percent of chord}\right]$$

Convex surface		Concave surface	
Station x	Ordinate y	Station x	Ordinate y
0	0	0	0
.161	.971	.839	-.371
.374	1.227	1.126	-.387
.817	1.679	1.683	-.395
1.981	2.599	3.019	-.367
4.399	4.035	5.601	-.243
6.868	5.178	8.132	-.090
9.361	6.147	10.639	.057
14.388	7.734	15.612	.342
19.477	8.958	20.553	.594
24.523	9.915	25.477	.825
29.611	10.640	30.389	1.024
34.706	11.153	35.294	1.207
39.804	11.479	40.196	1.373
44.904	11.598	45.096	1.542
50.000	11.488	50.000	1.748
55.087	11.139	54.913	2.001
60.161	10.574	59.839	2.278
65.214	9.801	64.786	2.559
70.245	8.860	69.755	2.804
75.256	7.808	74.744	2.932
80.242	6.607	79.758	2.945
85.204	5.272	84.796	2.804
90.154	3.835	89.846	2.369
95.096	2.237	94.904	1.555
100.068	.134	99.932	-.134
L.E. radius = 0.666 Slope through L.E. radius = 0.505			
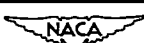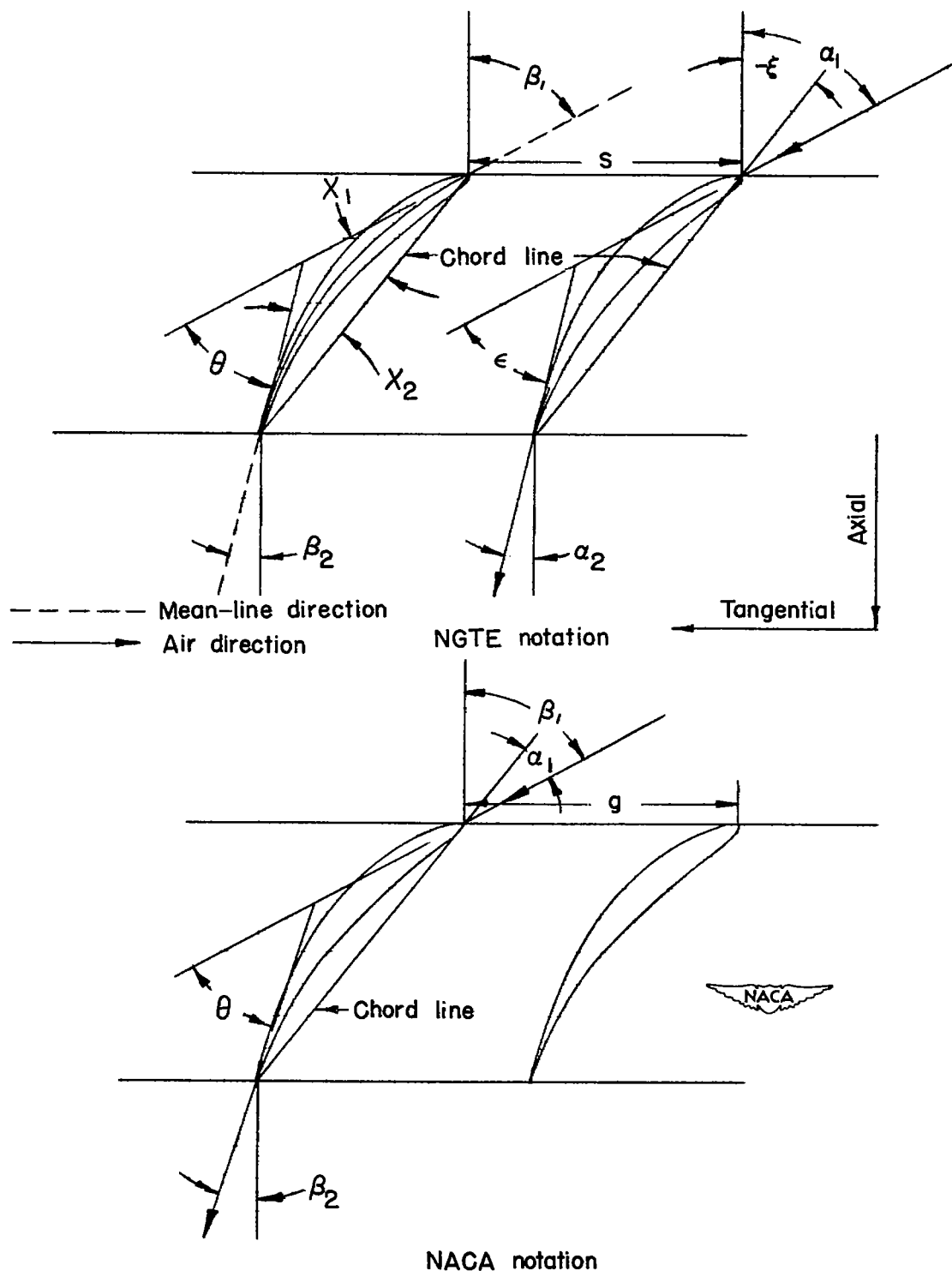
Figure 1.- Comparison of notations.
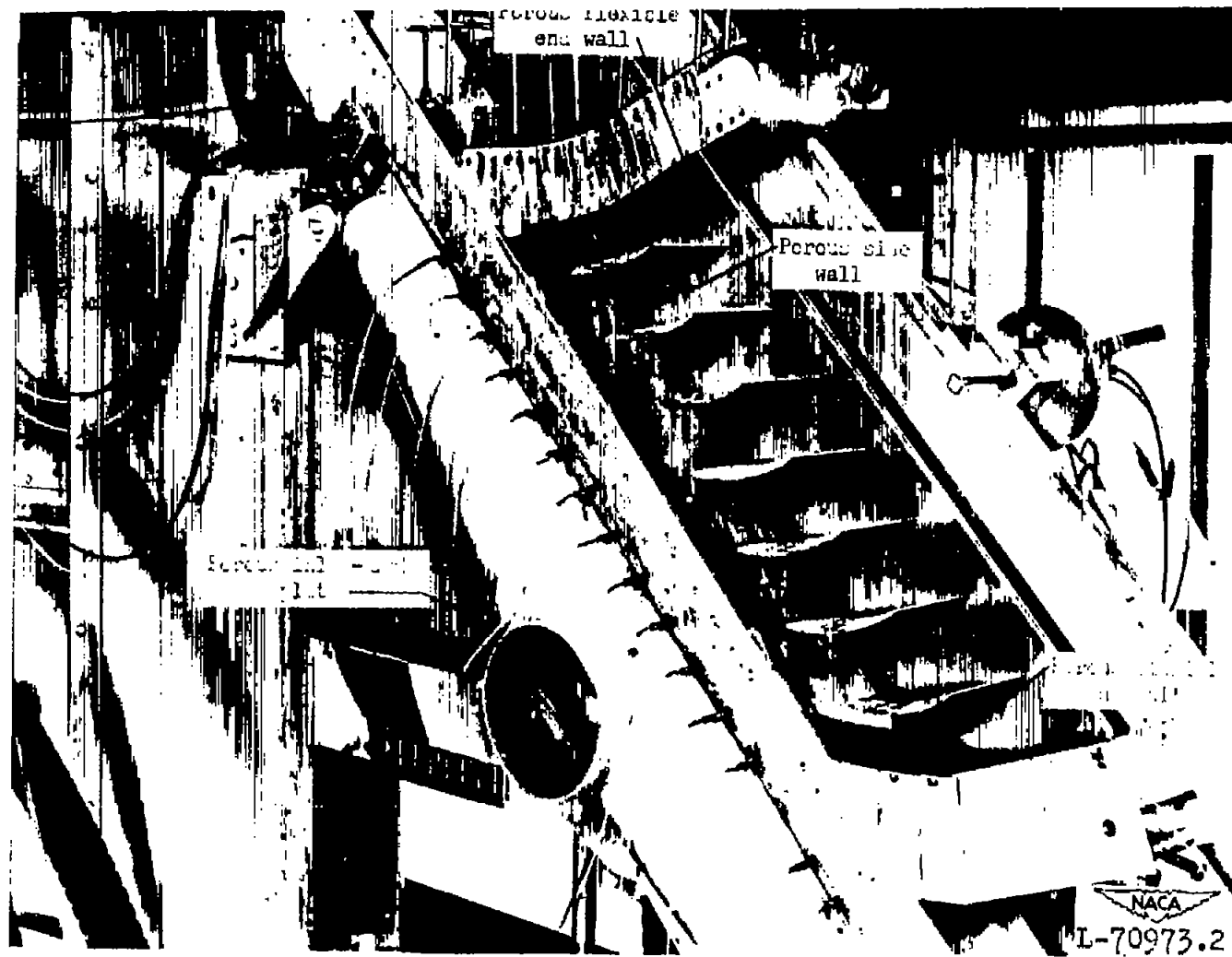
Figure 2.- Photograph of 5-inch cascade tunnel at the Langley Laboratory with portions removed to reveal the porous surfaces.

.0067 c L.E. rad.   .003 c T.E. thickness

$65\text{-}(12A_{10})10$

.012 c L.E. rad.   .006 c T.E. rad.
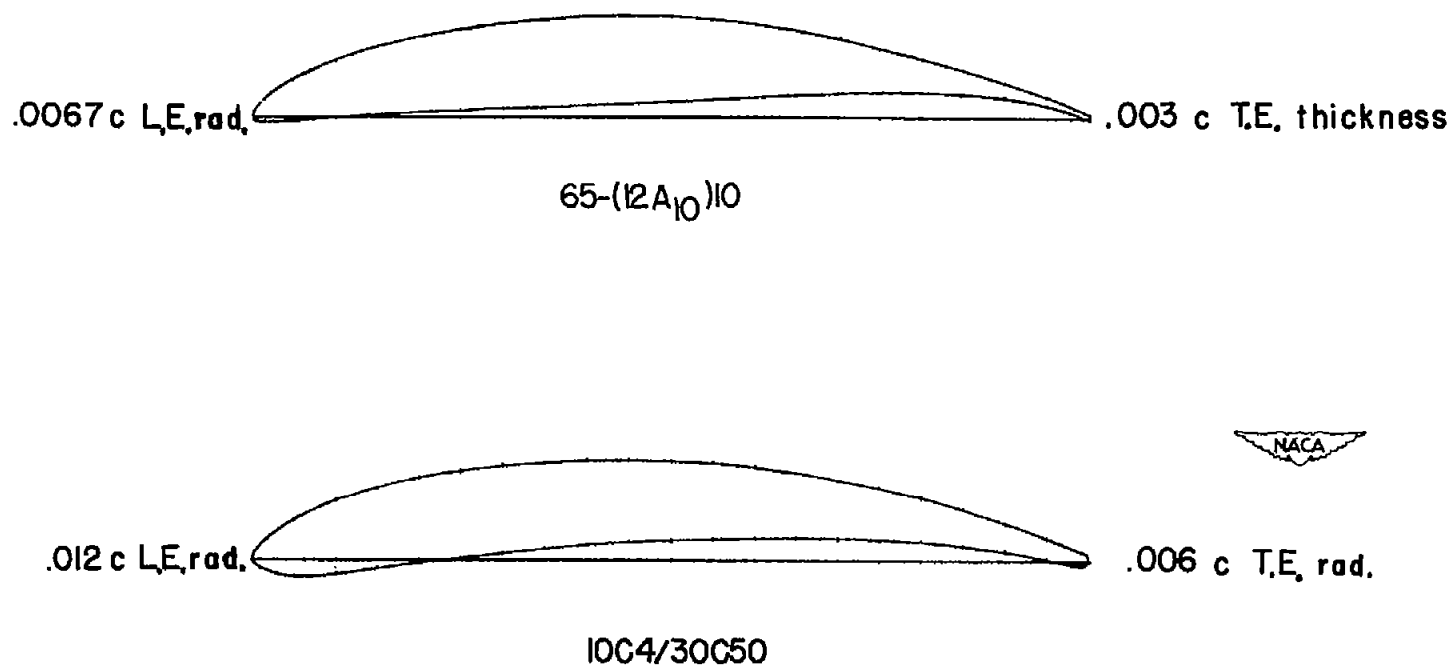
10C4/30C50

Figure 3.- NACA $65\text{-}(12A_{10})10$ and NGTE 10C4/30C50 compressor sections.
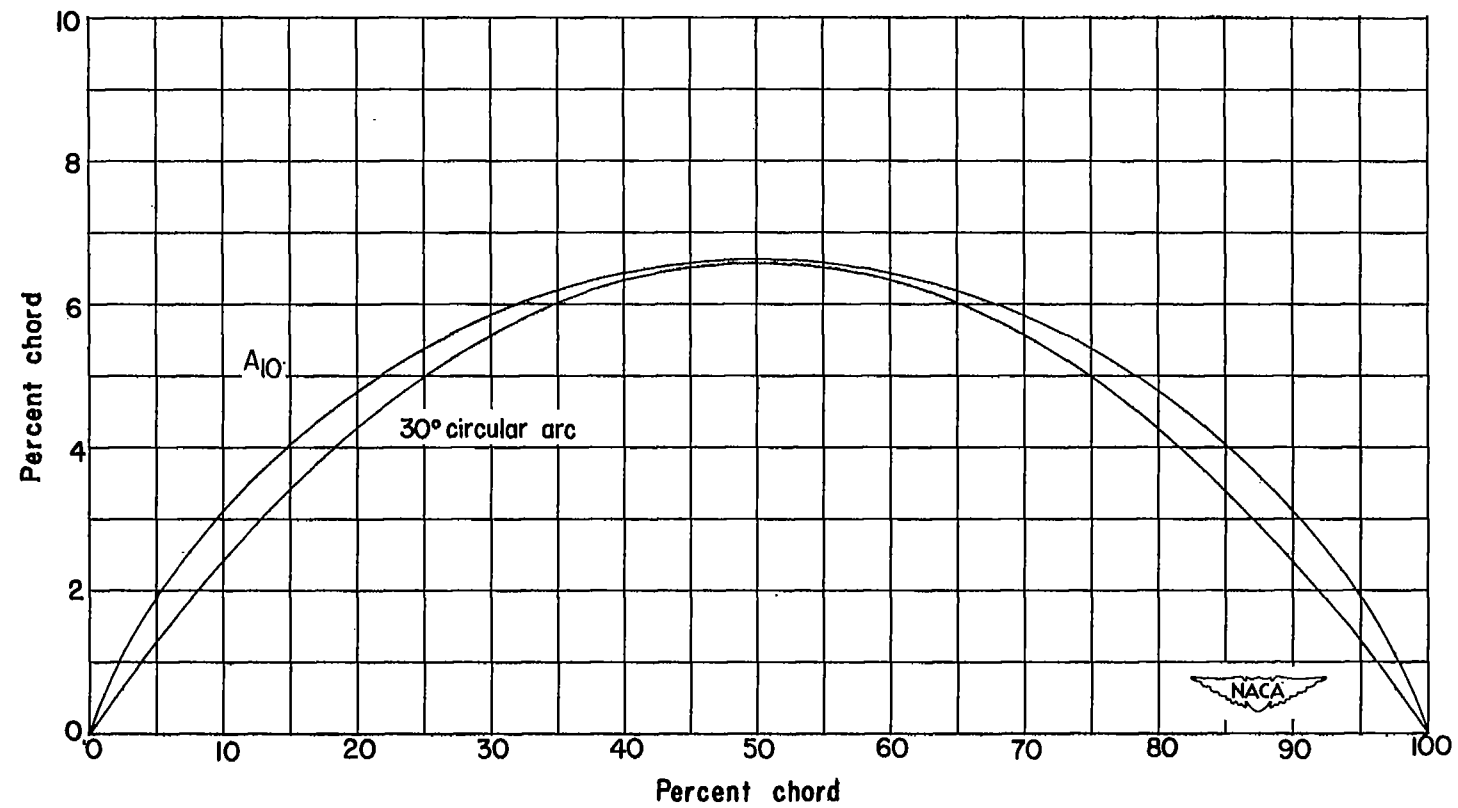
Figure 4.- Comparison of a 30° circular-arc mean line with an NACA constant-loading or A_{10} mean line having a $c_{l_o} = 1.2$.
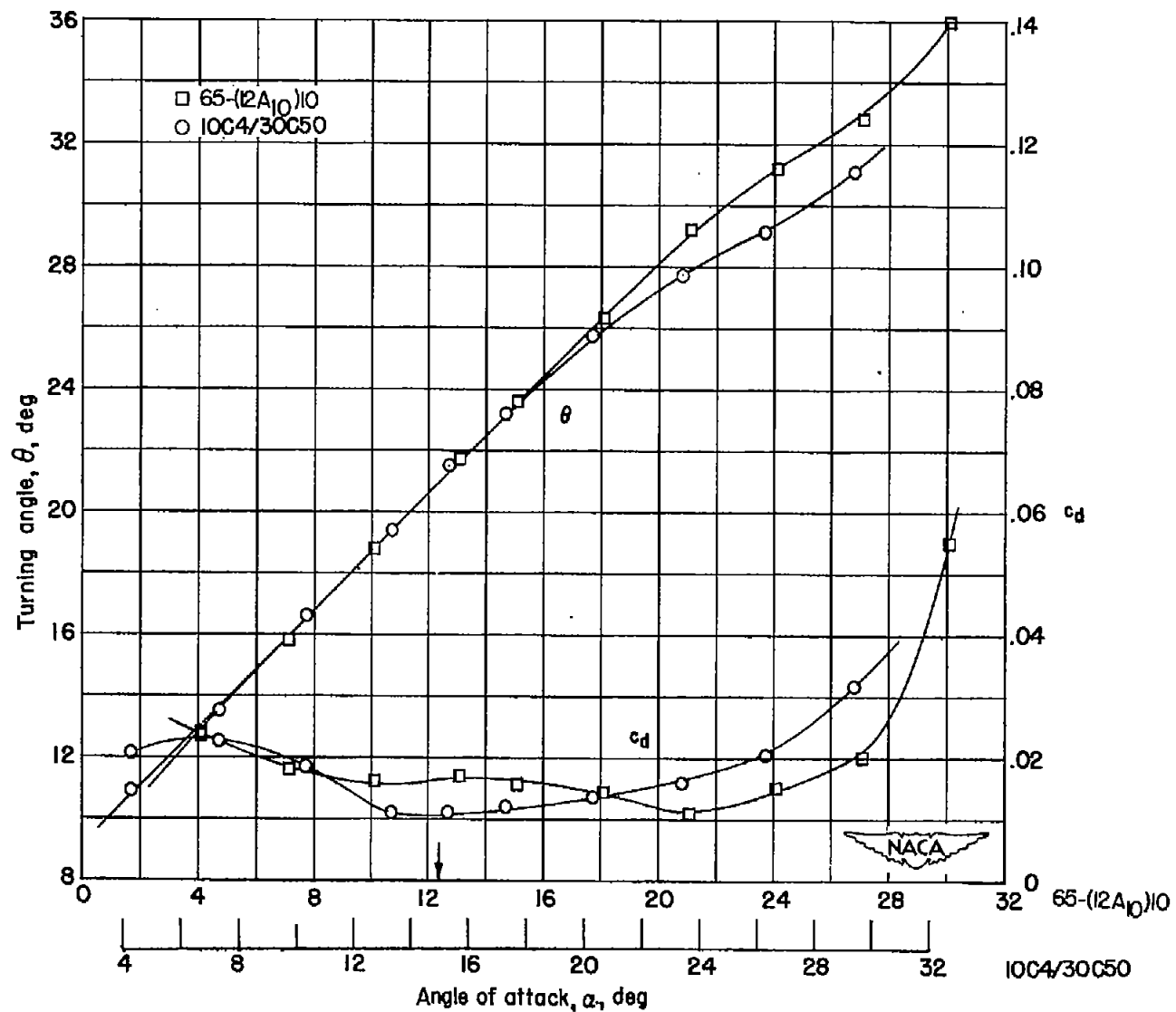
Figure 5.- Comparison of the characteristics of the NACA 65-(12A₁₀)10
and NGTE 10C4/30C50 sections at $\beta_1 = 30^0$ and $\sigma = 1.0$. Arrow indi-
cates design angle of attack.
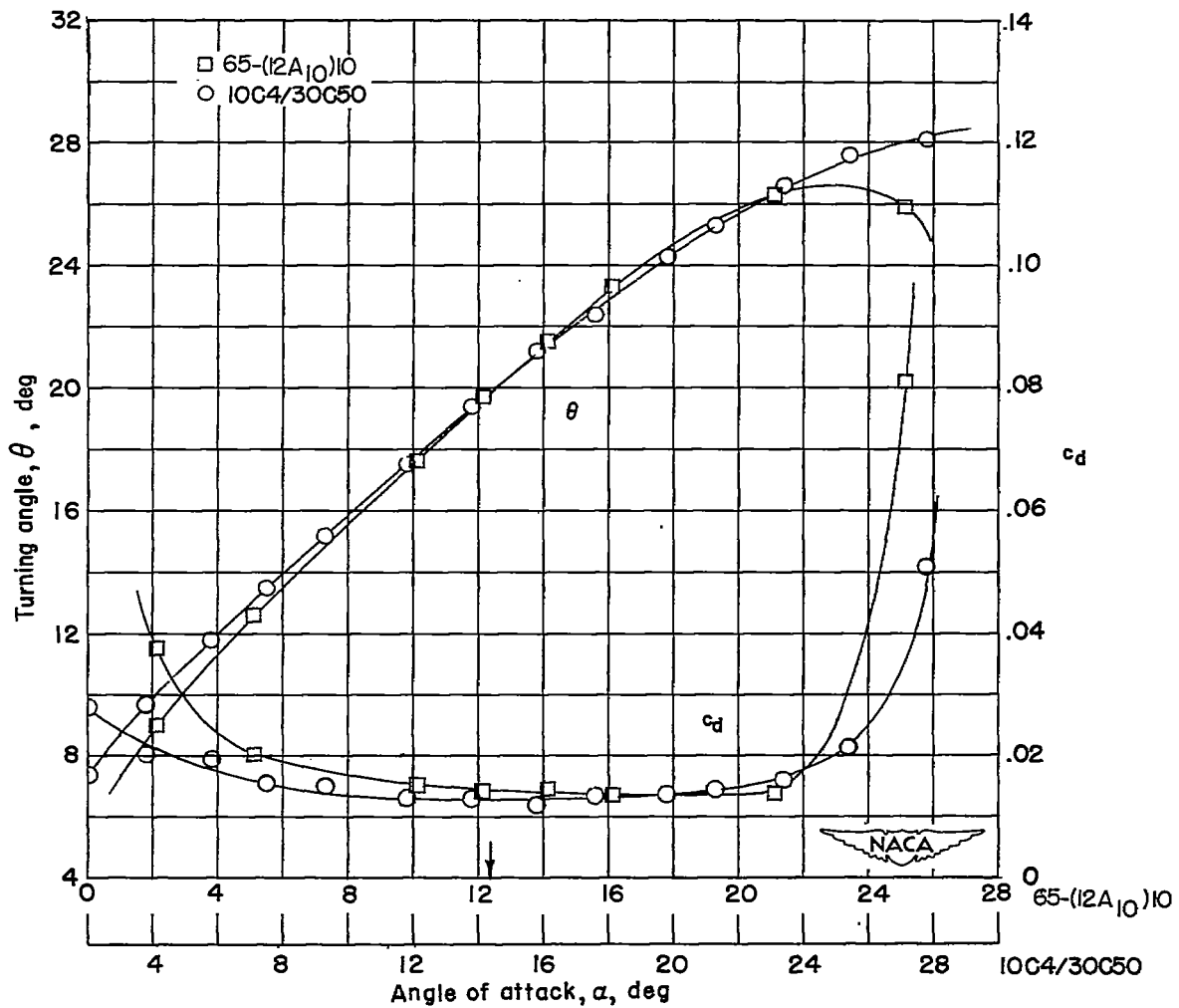
Figure 6.- Comparison of the characteristics of the NACA 65-(12A$_{10}$)10 and NGTE 10C4/30C50 sections at $\beta_1 = 45°$ and $\sigma = 1.0$. Arrow indicates design angle of attack.
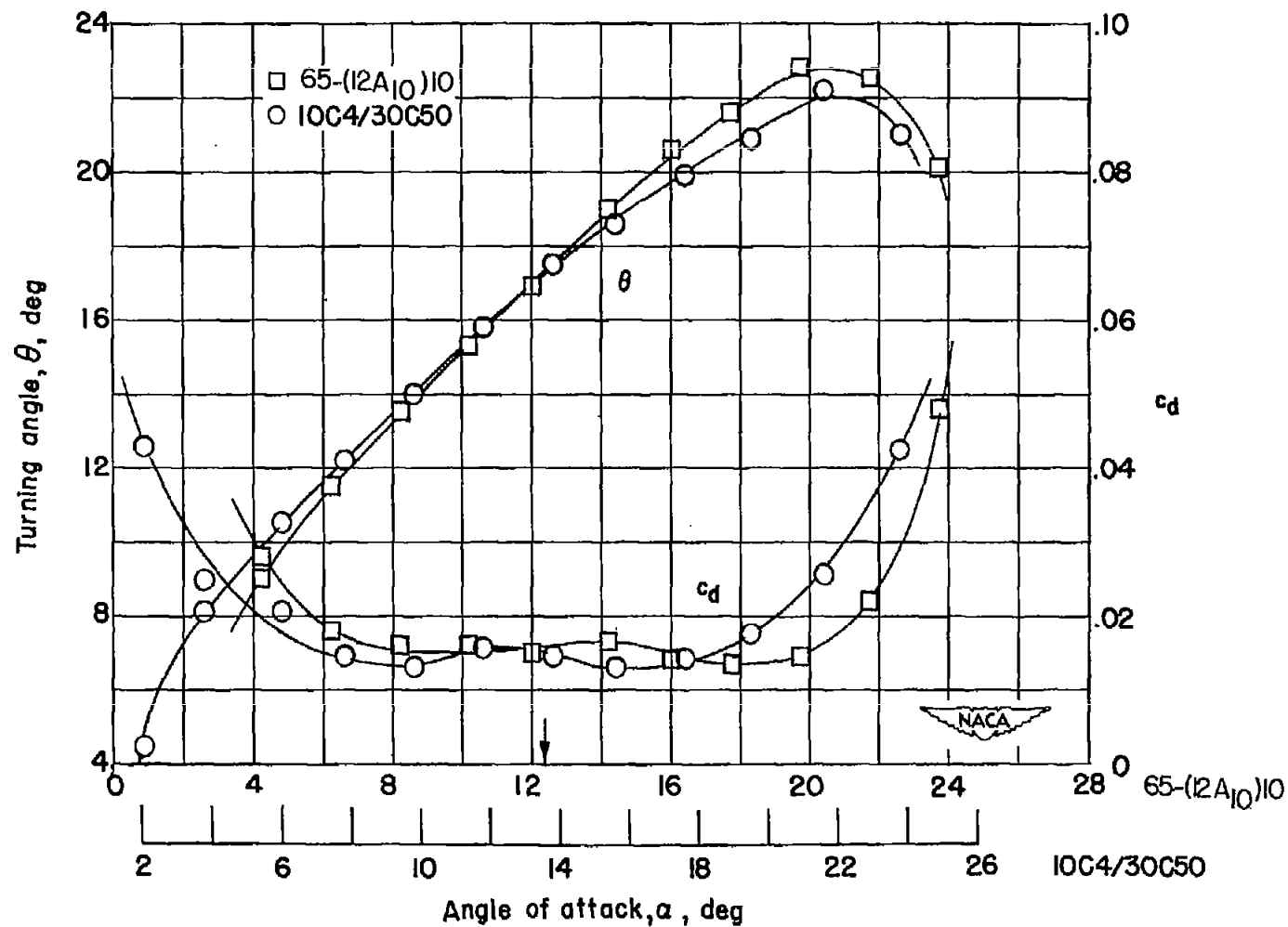
Figure 7.- Comparison of the section characteristics of the NACA 65-(12A$_{10}$)10 and NGTE 10C4/30C50 sections at $\beta_1 = 60°$ and $\sigma = 1.0$. Arrow indicates design angle of attack.
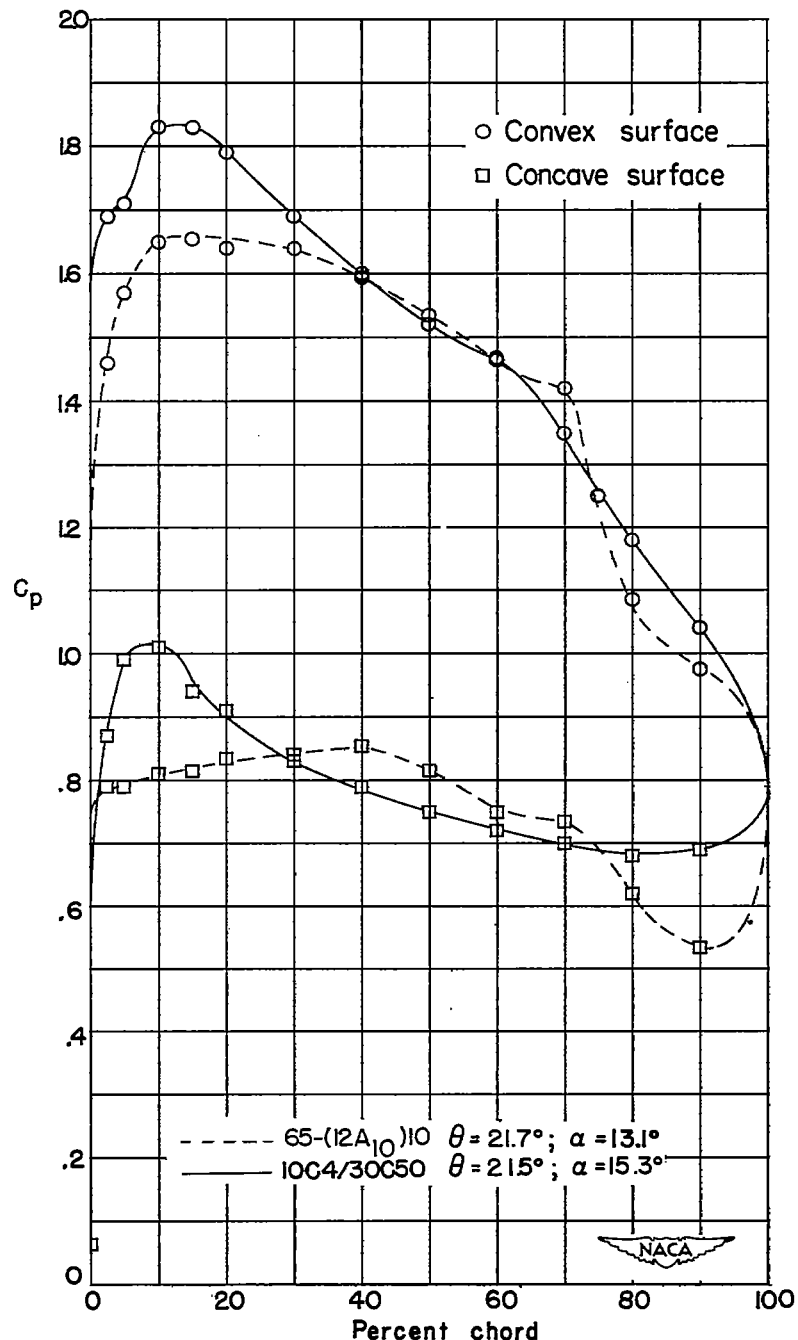
Figure 8.- Comparison of blade-surface pressure distributions of the NACA 65-(12A$_{10}$)10 and NGTE 10C4/30C50 sections at $\beta_1 = 30^\circ$ and $\sigma = 1.0$.
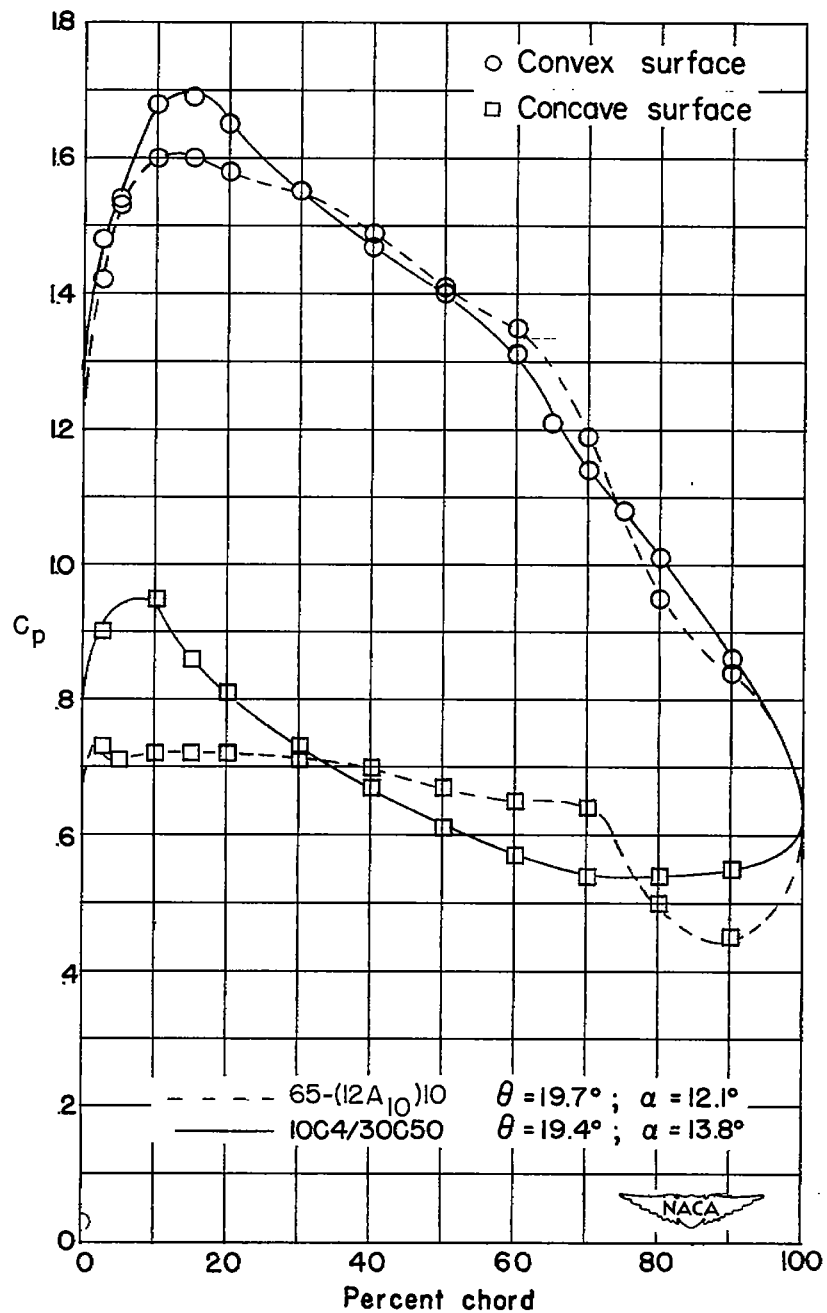
Figure 9.- Comparison of blade-surface pressure distributions of the
NACA 65-(12A₁₀)10 and NGTE 10C4/30C50 sections at $\beta_1 = 45°$ and
$\sigma = 1.0$.
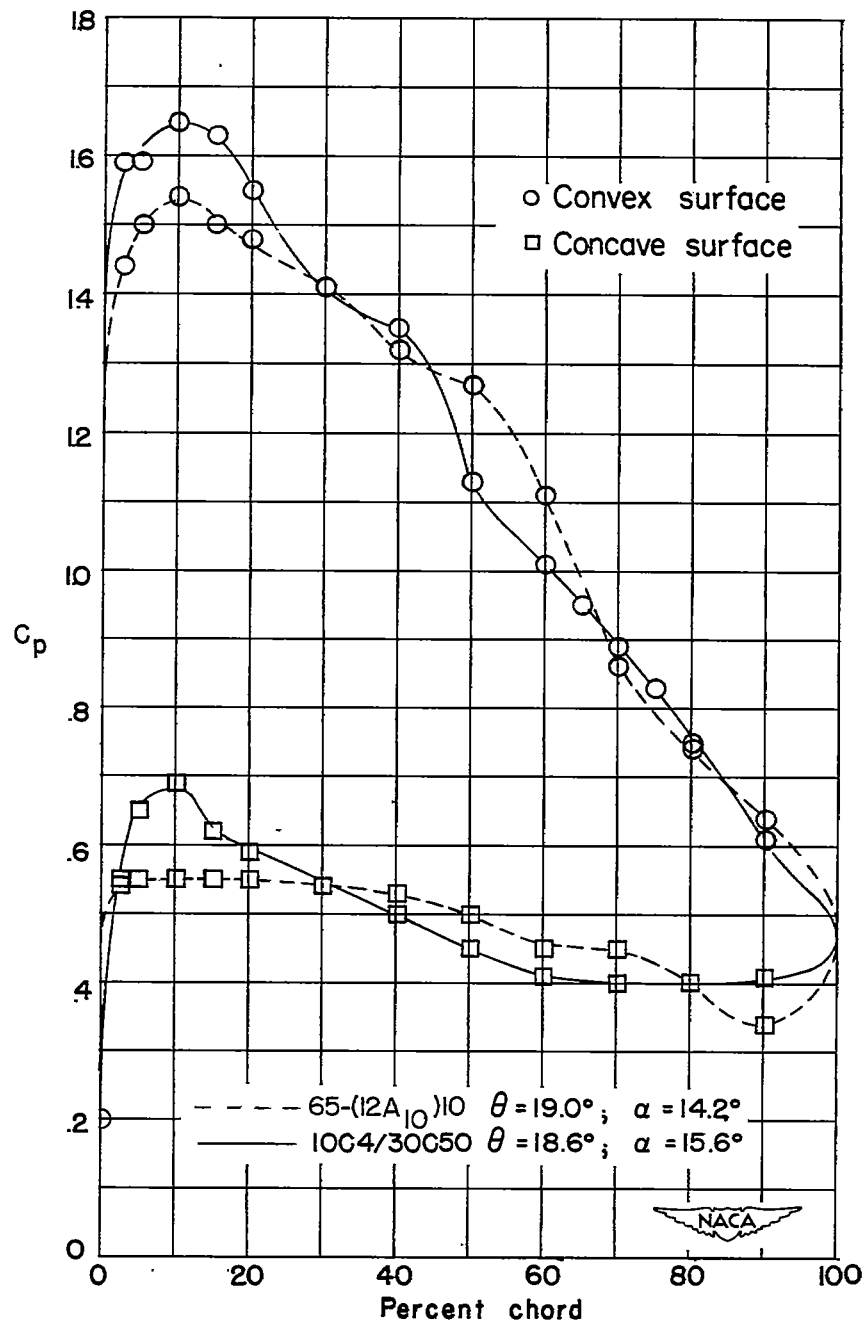
Figure 10.- Comparison of blade-surface pressure distributions of the
NACA 65-($12A_{10}$)10 and NGTE 10C4/30C50 sections at $\beta_1 = 60°$ and
$\sigma = 1.0$.
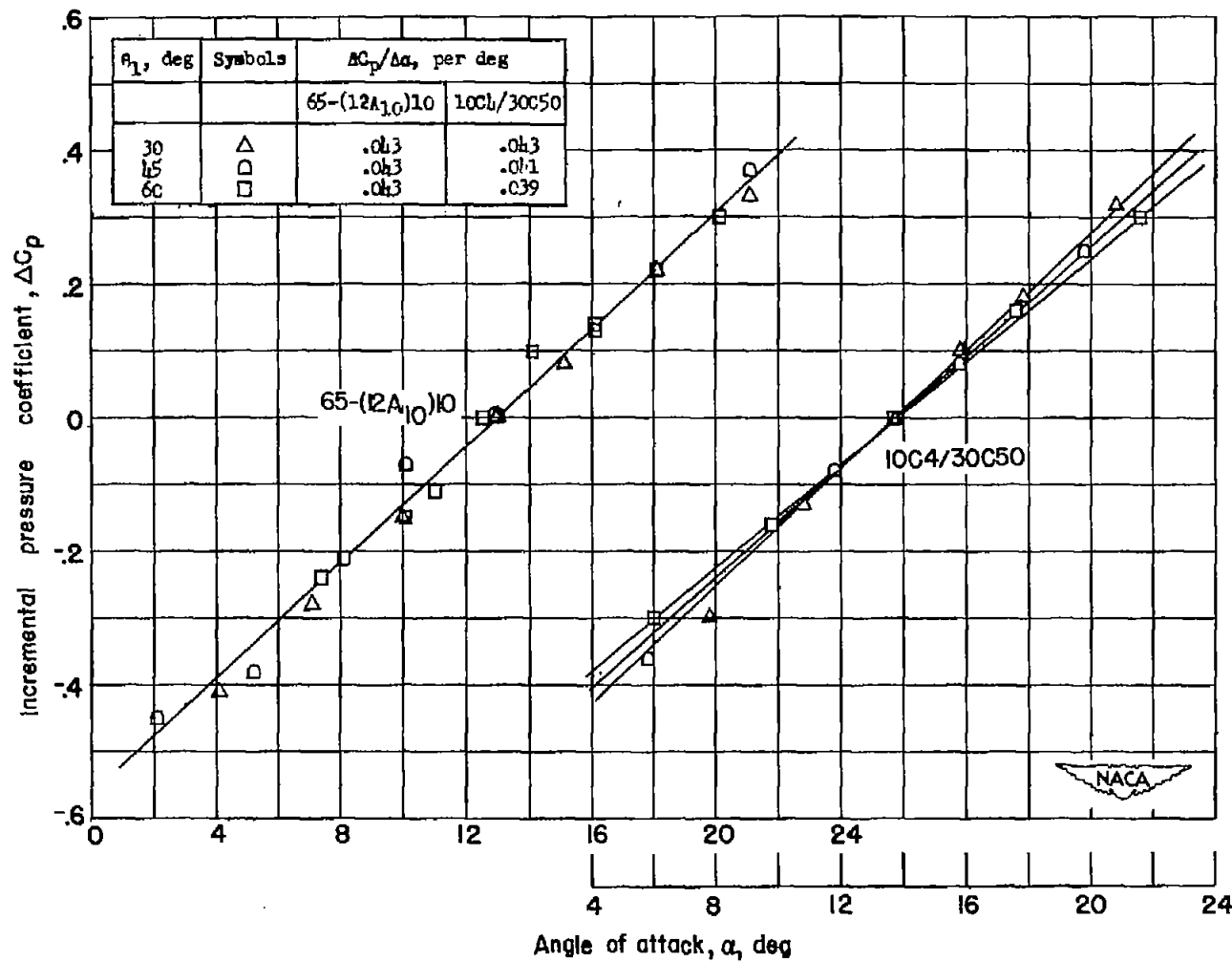
Figure 11.- Variation of the incremental pressure coefficient ΔC_p with angle of attack α for NACA 65-(12A$_{10}$)10 and NGTE 10C4/30C50 blade sections at 10-percent-chord station on convex surface. $\sigma = 1.0$.
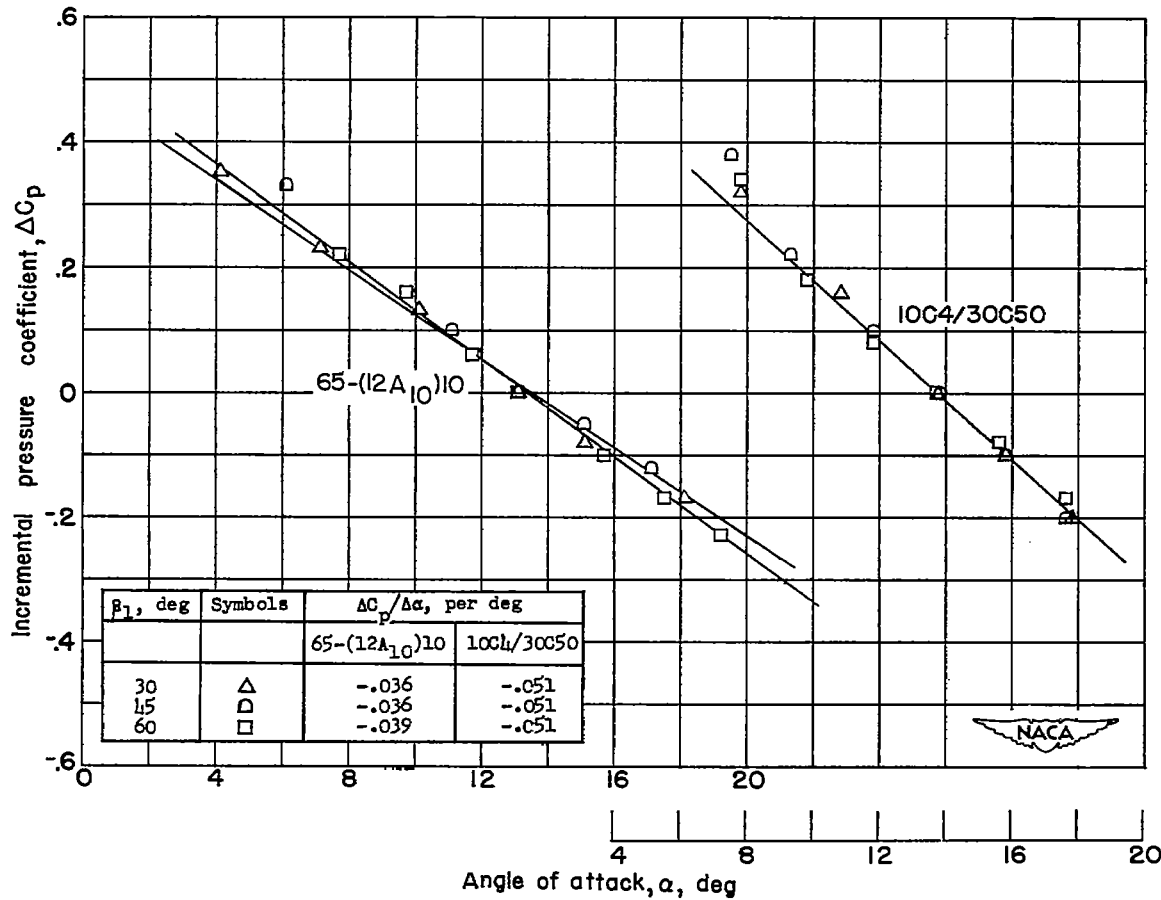
Figure 12.- Variation of the incremental pressure coefficient ΔC_p with angle of attack α for the NACA 65-(12A$_{10}$)10 and NGTE 10C4/30C50 blade sections at the 10-percent-chord station on the concave surface. $\sigma = 1.0$.
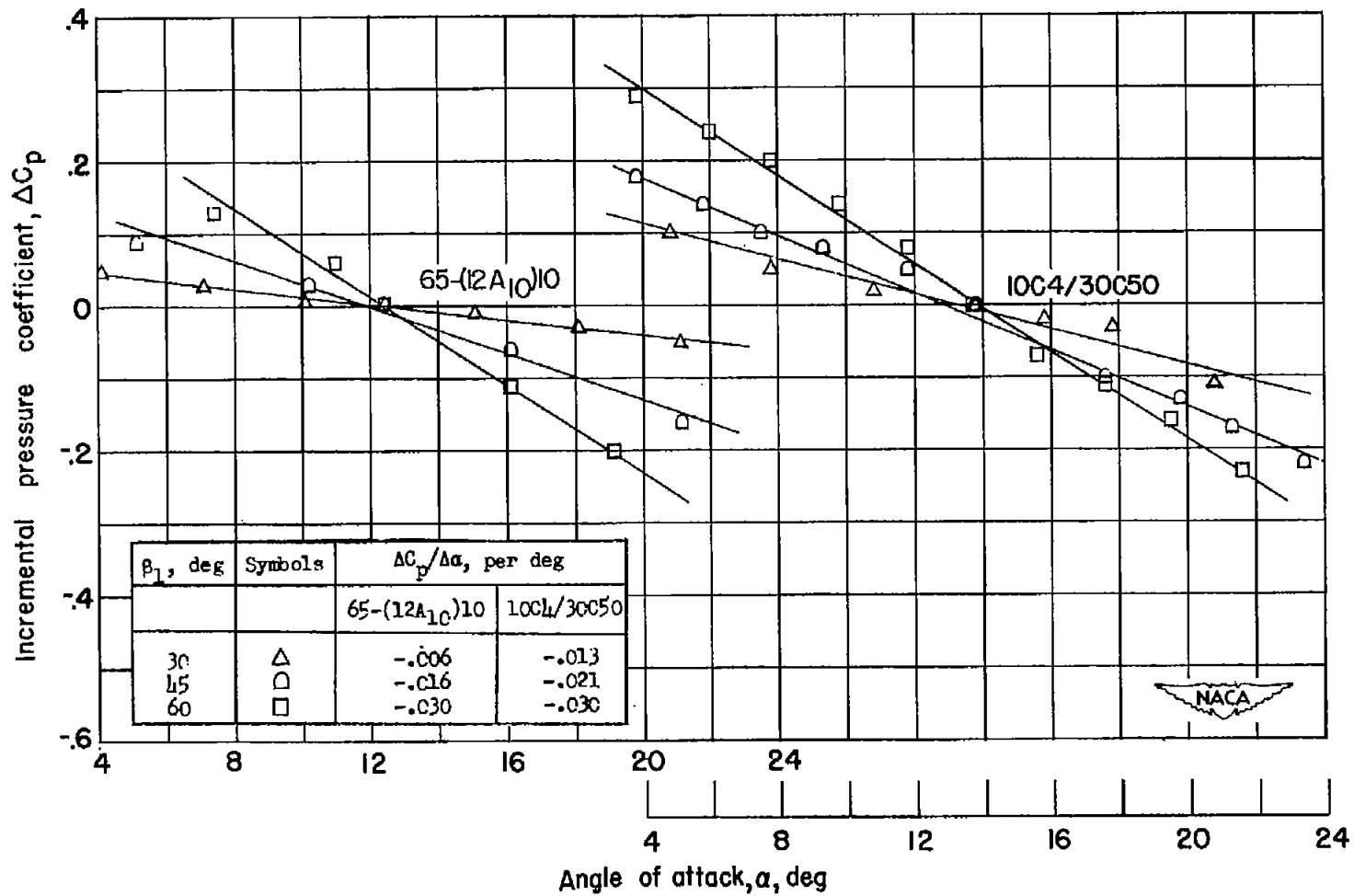
Figure 13.- Variation of the incremental pressure coefficient ΔC_p with angle of attack α for NACA 65-(12A$_{10}$)10 and NGTE 10C4/30C50 blade sections at 60-percent-chord station on convex surface. $\sigma = 1.0$.
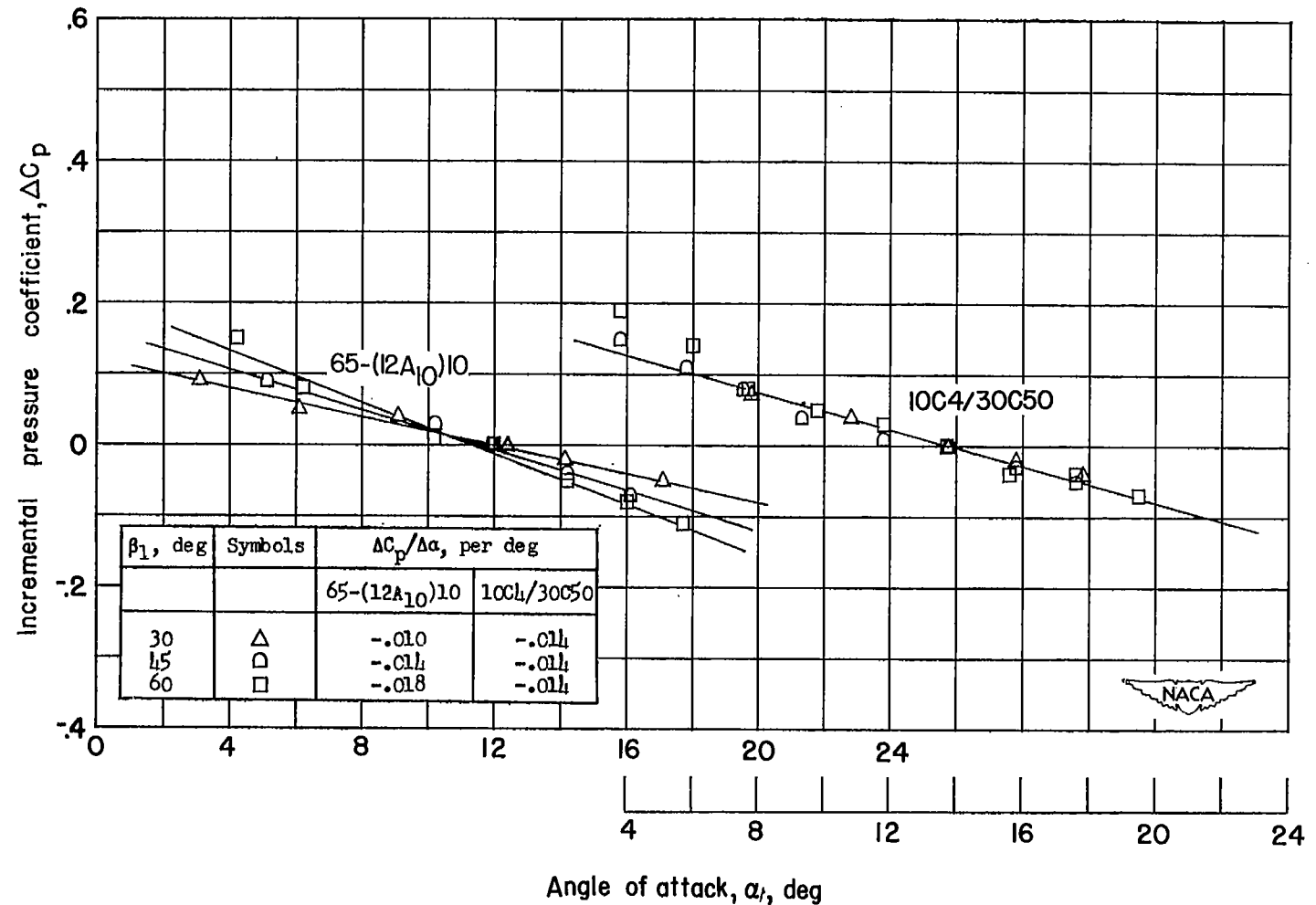
Figure 14.- Variation of the incremental pressure coefficient ΔC_p with angle of attack α for NACA 65-$(12A_{10})$10 and NGTE 10C4/30C50 blade sections at the 60-percent-chord station on the concave surface. $\sigma = 1.0$.
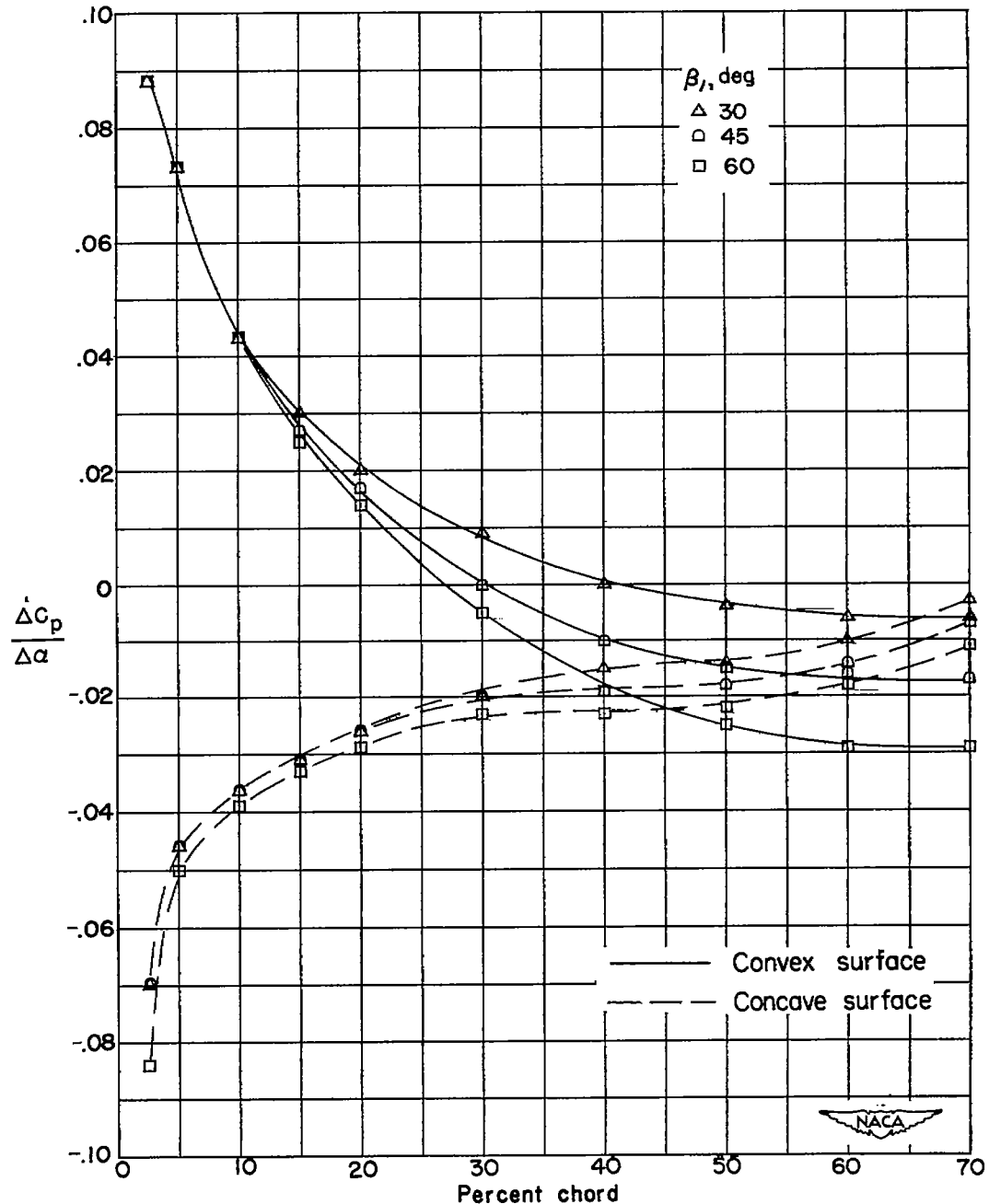
Figure 15.- Chordwise variation of the slope $\Delta C_p/\Delta \alpha$ for the NACA 65-(12A$_{10}$)10 blade section at $\beta_1 = 30°$, 45°, and 60°. $\sigma = 1.0$.
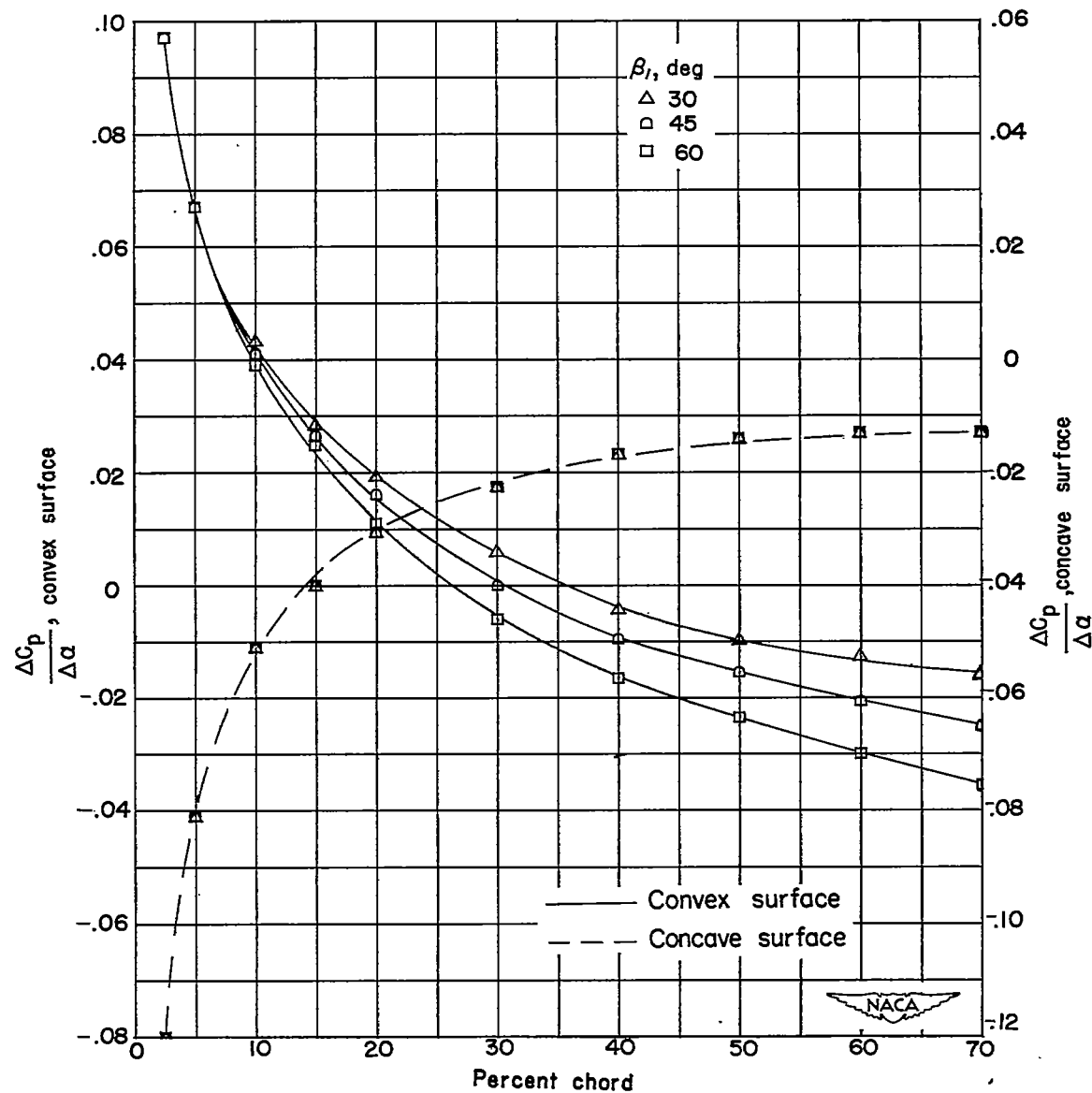
Figure 16.- Chordwise variation of the slope $\Delta C_p/\Delta\alpha$ for the NGTE 10C4/30C50 blade section at $\beta_1 = 30°$, 45°, and 60°. $\sigma = 1.0$.
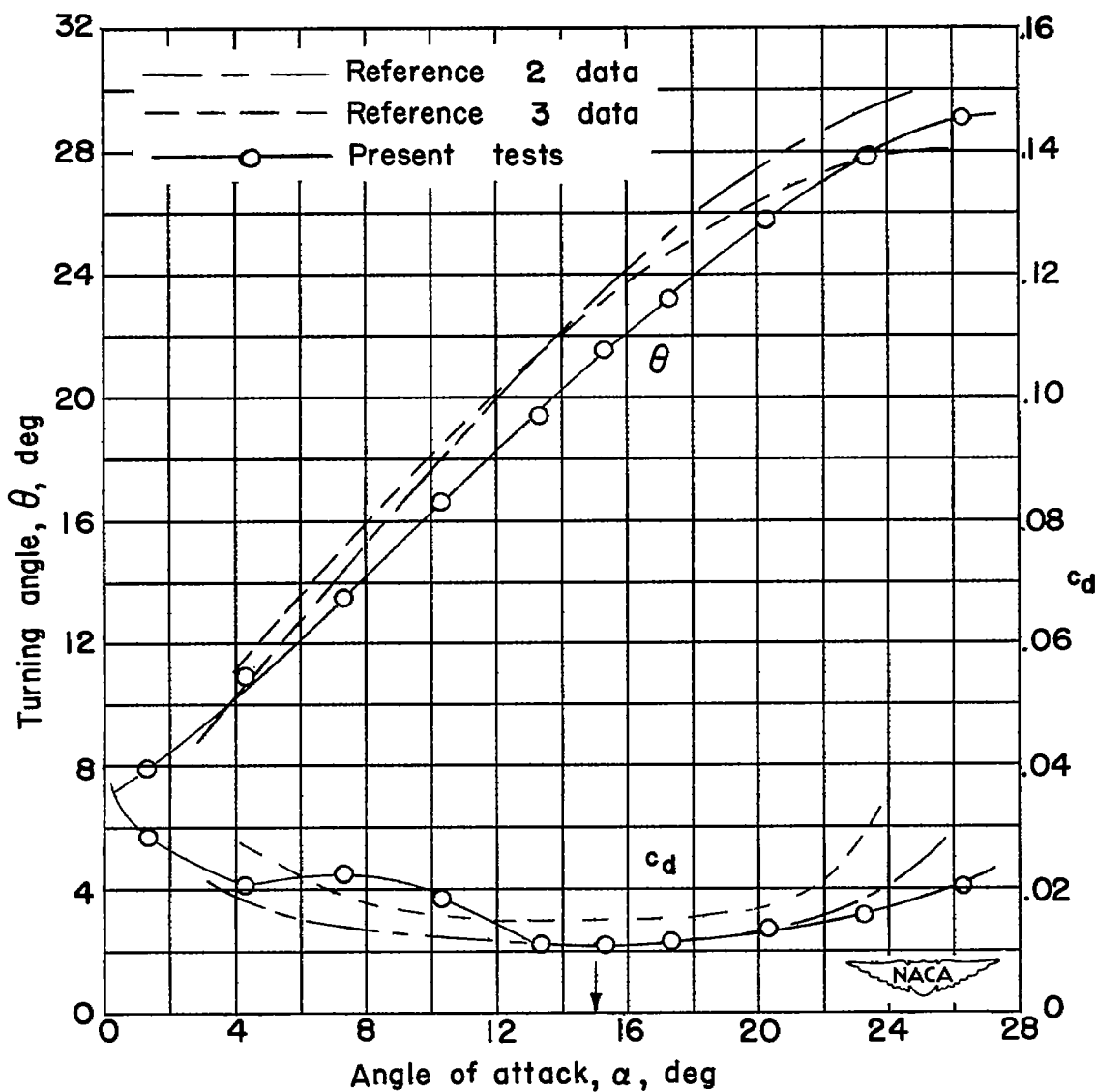
Figure 17.- Section characteristics of NGTE 10C4/30C50 section at $\beta_1 = 30^\circ$ and $\sigma = 1.0$. Arrow indicates design angle of attack.
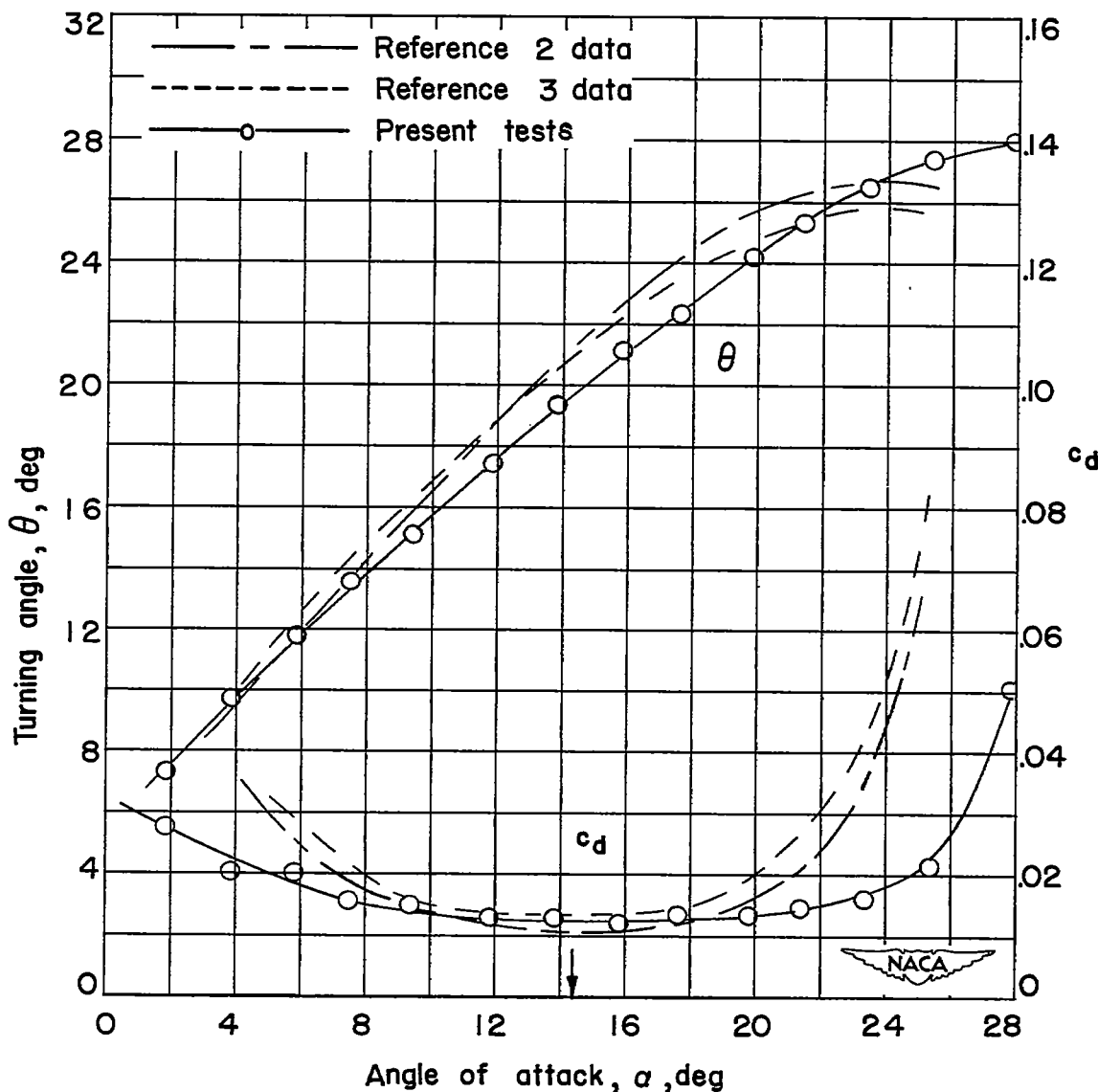
Figure 18.- Section characteristics of NGTE 10C4/30C50 section at $\beta_1 = 45^\circ$ and $\sigma = 1.0$. Arrow indicates design angle of attack.
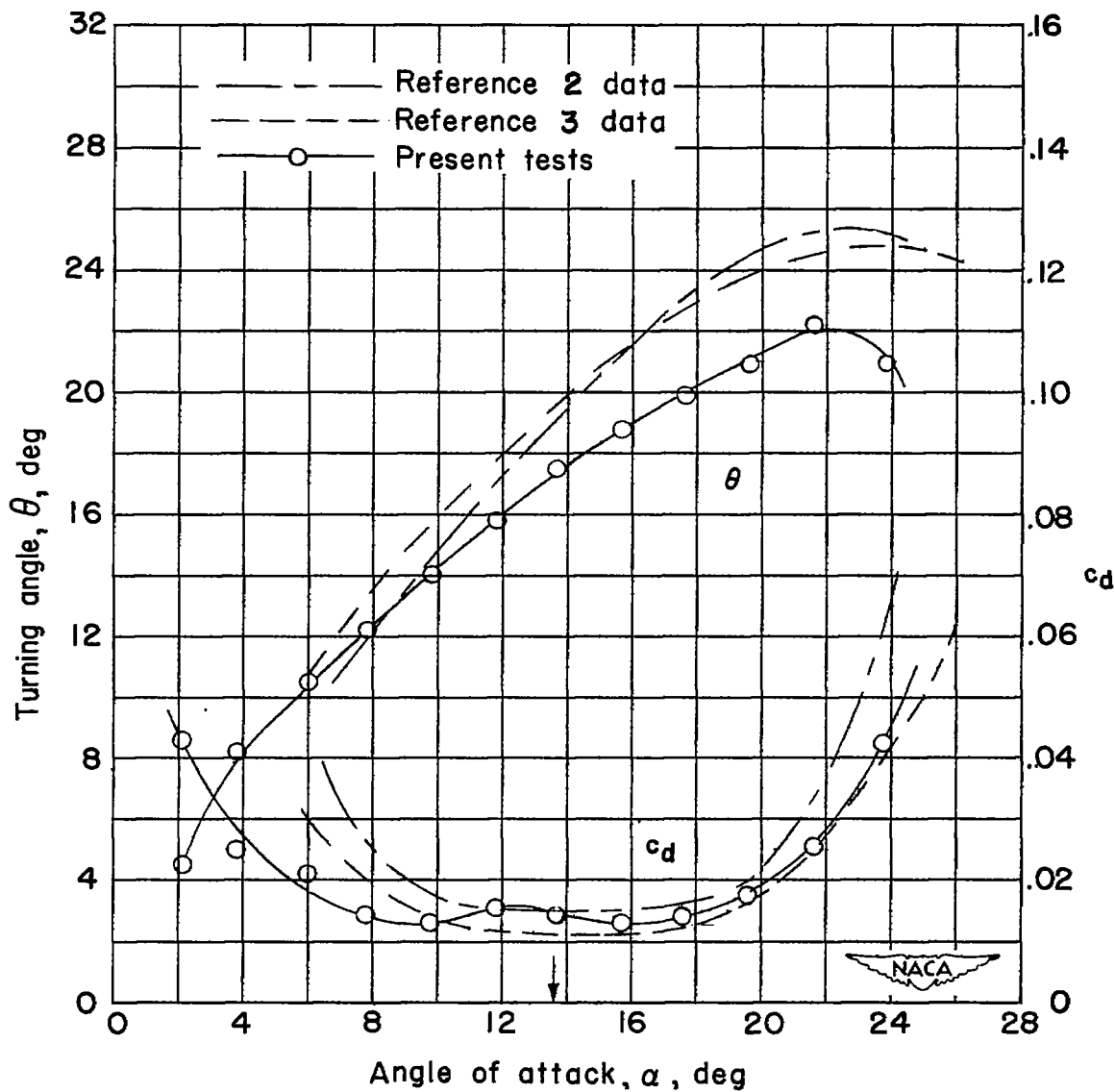
Figure 19.- Section characteristics of NGTE 10C4/30C50 section at
$\beta_1 = 60°$ and $\sigma = 1.0$. Arrow indicates design angle of attack.
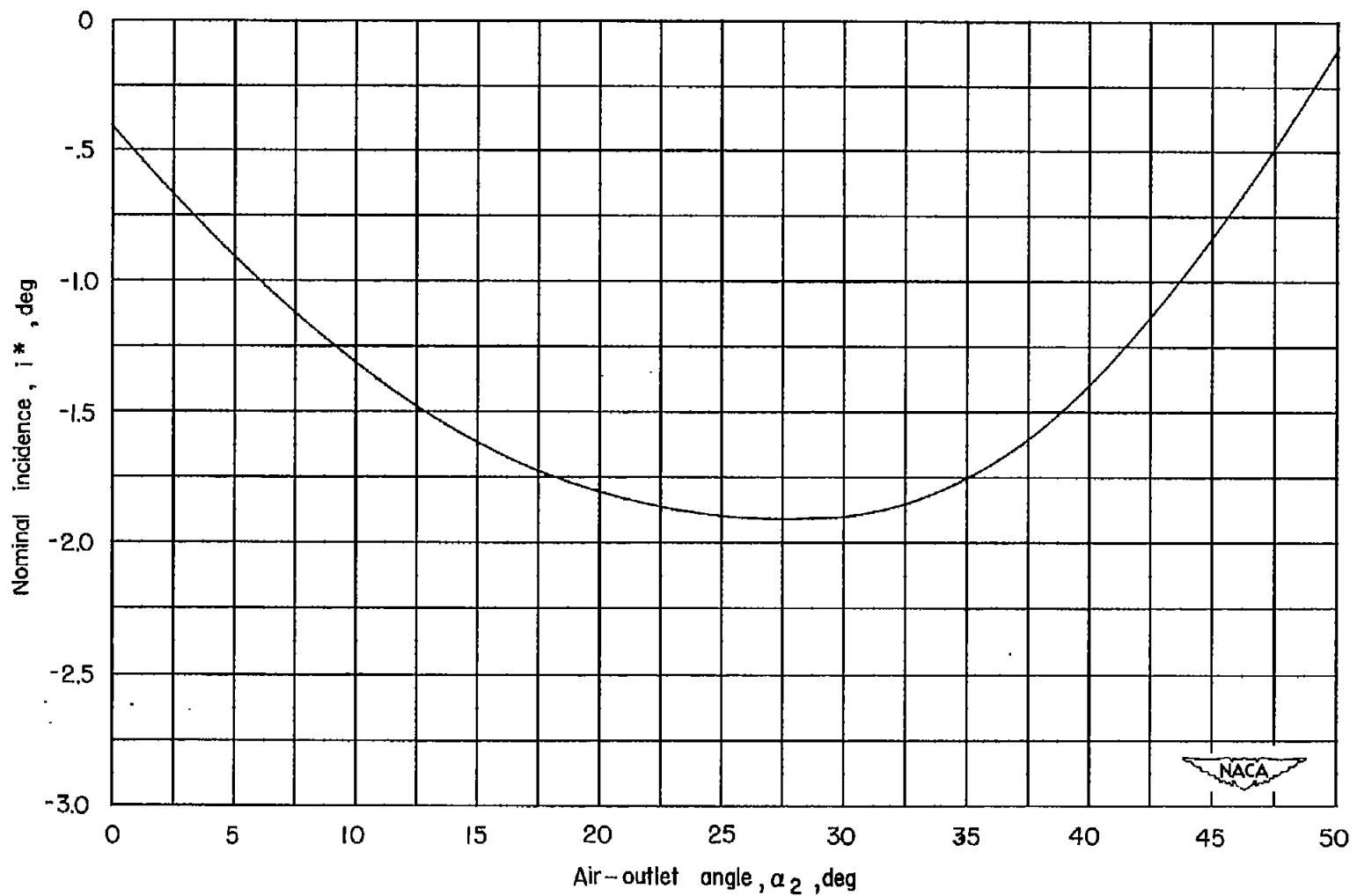
Figure 20.- Variation of nominal incidence with air-outlet angle for
NGTE 10C4/3050 section (ref. 3).
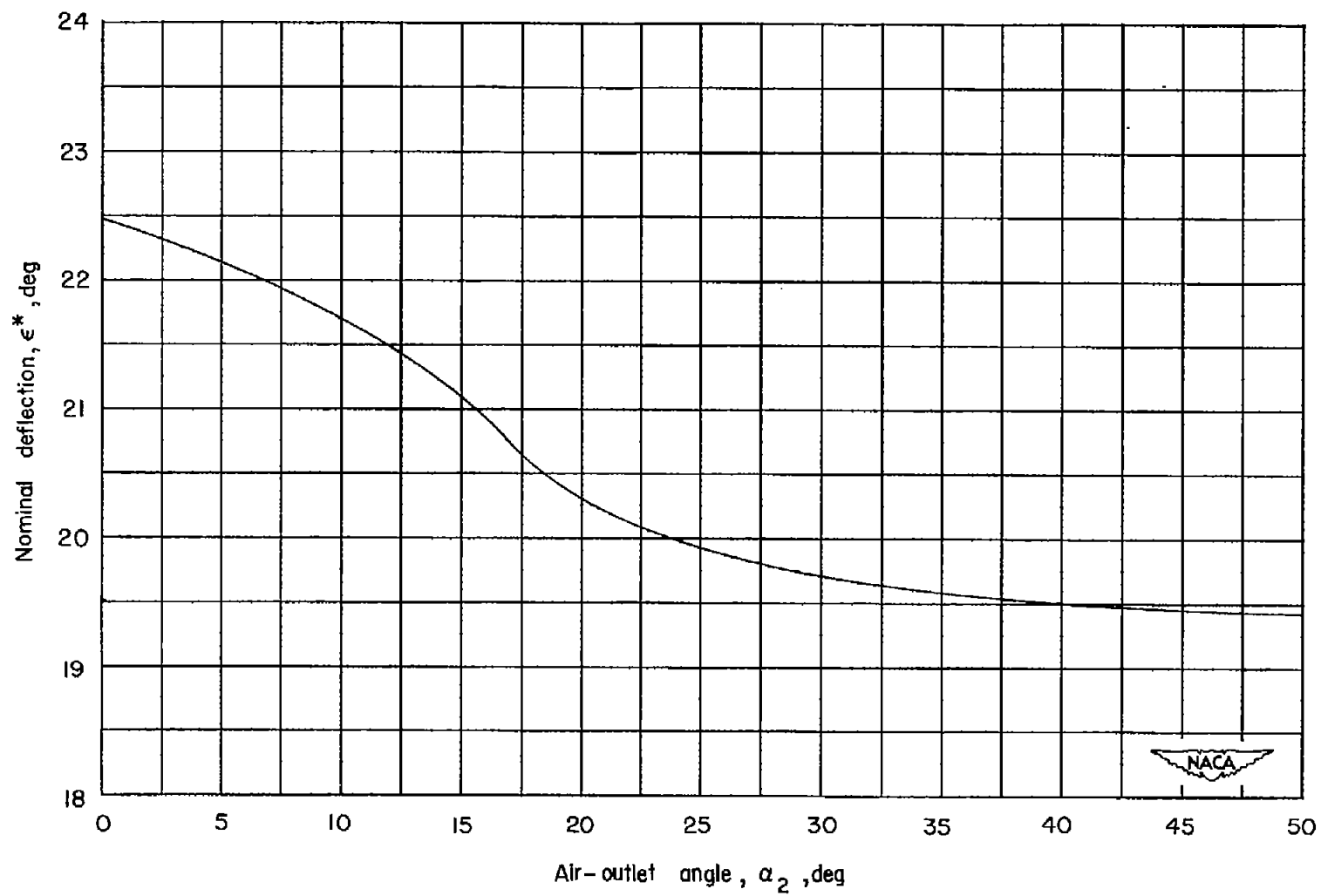
Figure 21.- Variation of nominal turning angle with air-outlet angle for
NGTE 10C4/30C50 section (ref. 3).